Adaptive Phase Estimation with Squeezed Vacuum Approaching the Quantum Limit

M. A. Rodríguez-García and F. E. Becerra

Center for Quantum Information and Control, Department of Physics and Astronomy, University of New Mexico, Albuquerque, New Mexico 87131, USA

Phase estimation plays a central role in communications, sensing, and information processing. Quantum correlated states, such as squeezed states, enable phase estimation beyond the shot-noise limit, and in principle approach the ultimate quantum limit in precision, when paired with optimal quantum measurements. However, physical realizations of optimal quantum measurements for optical phase estimation with quantum-correlated states are still unknown. Here we address this problem by introducing an adaptive Gaussian measurement strategy for optical phase estimation with squeezed vacuum states that, by construction, approaches the quantum limit in precision. This strategy builds from a comprehensive set of locally optimal POVMs through rotations and homodyne measurements and uses the Adaptive Quantum State Estimation framework for optimizing the adaptive measurement process, which, under certain regularity conditions, guarantees asymptotic optimality for this quantum parameter estimation problem. As a result, the adaptive phase estimation strategy based on locally-optimal homodyne measurements achieves the quantum limit within the phase interval of $[0, \pi/2)$. Furthermore, we generalize this strategy by including heterodyne measurements, enabling phase estimation across the full range of phases from $[0, \pi)$, where squeezed vacuum allows for unambiguous phase encoding. Remarkably, for this phase interval, which is the maximum range of phases that can be encoded in squeezed vacuum, this estimation strategy maintains an asymptotic quantum-optimal performance, representing a significant advancement in quantum metrology.

1 Introduction

Quantum metrology uses the quantum properties of physical systems to enhance the measurement precision of physical quantities beyond the classical limits [1, 2]. Quantum mechanics states that all physical observables are represented by self-adjoint operators on a Hilbert space. As such, the measurement of a physical quantity of a system involves projecting the quantum state of such system onto one of the eigenspaces of the corresponding self-adjoint operator. However, certain physical quantities, such as time, phase, or temperature, lack an associated self-adjoint operator [3, 4]. Consequently, to determine the values of these physical quantities, it is necessary to measure some observables of the system and estimate their values from the observed results. This process is referred to as quantum parameter estimation [3, 4].

Among different parameter estimation problems, the problem of phase estimation is ubiquitous in many areas of physics and engineering including, but not limited to, gravitational wave detection [5], quantum imaging [6], atomic clocks [7], magnetometry [8], and quantum information processing [9]. However, the performance of traditional phase estimation methods is limited by the fundamental properties of the physical states carrying the phase information. The maximum achievable precision for phase estimation for probe states that lack quantum correlations, typically used for phase estimation, is defined as shot-noise limit (SNL) [1, 10].

Numerous methods have been developed for achieving phase estimation beyond the SNL by exploiting probe states with inherent quantum correlations. Among different types of quantum correlations, entanglement holds a significant potential for improving precision in phase estimation. Nevertheless, highly entangled states used for phase estimation, such as NOON states, are delicate and can be readily disrupted by loss, environmental noise, and decoherence, thereby limiting their practicality for real world applications [11–14]. In this regard, squeezed state probes offer a more viable alternative for robust phase estimation [15, 16]. Squeezed states allow for reducing the quantum noise in one observable below the SNL at the expense of an increased noise in another non-commuting observable. This reduction in quantum noise can significantly enhance the precision of phase measurements [5, 7, 16, 17], and is a valuable resource for enabling robust optical quantum metrology and phase estimation.

Advances in photonic quantum technologies for phase estimation and quantum metrology have yielded squeezed light sources with a high degree of

squeezing [18–21]. Moreover, experimental demonstrations of quantum metrology and sensing utilizing squeezed optical probes have achieved sensitivities surpassing the SNL [5, 22–24]. However, there remain significant challenges in devising optimal estimation strategies, including optimal measurements and estimators, that can efficiently attain the ultimate quantum limit of precision for any optical phase estimation problem.

A noteworthy measurement approach for optical phase estimation with squeezed states is the homodyne measurement. This measurement has the potential for reaching the quantum limit for a specific, optimized phase when a predetermined level of squeezing is present in the probe state [25]. However, this optimal phase must be known beforehand in order to reach the quantum limit, making this approach impractical. To overcome this limitation, two-step adaptive methods for phase estimation allow for increasing the range of phases within $[0, \pi/2)$ for which estimation below the SNL is possible [25, 26]. These methods can approximate the quantum limit in precision in the asymptotic limit of many input states for phases around this optimal phase. However, as the input phase deviates from the predetermined optimal phase of homodyne, these estimation strategies show a considerable discrepancy with the quantum limit.

In this work, we theoretically demonstrate a multistep adaptive Gaussian measurement strategy for optical phase estimation with squeezed vacuum states that, by construction, approaches the quantum limit in precision with a fast convergence rate for any phase encoded in squeezed vacuum. This estimation strategy uses homodyne measurements to implement a comprehensive set of locally optimal POVMs (Positive Operator Value Measures). Then the strategy performs adaptive optimization based on the Adaptive Quantum State Estimation (AQSE) framework to ensure the asymptotic consistency and efficiency of the estimator of the optical phase [27]. Based on rigorous mathematical analysis, we prove that this adaptive strategy approaches the quantum limit for phases within $[0, \pi/2)$ in the asymptotic limit of many adaptive steps. Furthermore, we generalize this strategy to incorporate heterodyne sampling making it possible to extend the parametric range to $[0, \pi)$, which is the maximum range of phases that can be encoded in squeezed vacuum. We show that this combined homodyne-heterodyne strategy maintains an asymptotic quantum optimal performance.

The paper is organized as follows: In Sec. 2 we provide a concise overview of the theory of single parameter estimation. Then, we discuss the problem of optical phase estimation in the context of quantum systems, followed by an overview of phase estimation with squeezed states. In Sec. 3, we describe the proposed optimal phase estimation strategy based on adaptive Gaussian measurements with squeezed vacuum states. By leveraging homodyne measurements and rotations, we construct a collection of locally optimal POVMs, which allows us to apply the mathematical framework of AQSE to Gaussian measurements and feedback [27, 28]. Through formal mathematical analysis, we show that this adaptive measurement process allows for extracting the maximum possible information pertaining to the phase encoded in squeezed vacuum states in the asymptotic regime. Appendix 8.2 gives a mathematical proof of the asymptotic optimality of the adaptive strategy, showing its convergence to the quantum Cramér-Rao lower bound (QCRB). In Sec. 4, we use numerical simulations to evaluate the performance of this strategy, and investigate its performance under losses and system imperfections in Sec. 5. We observe that this strategy approaches the quantum limit for phases within $[0, \pi/2)$, outperforming previous phase estimation strategies. Sec. 6, describes the combined homodyne-heterodyne strategy for phase estimation in the full range for squeezed vacuum of $[0, \pi)$, and the proof of its asymptotic optimality in Appendix 8.4. Finally, Sec. 7 contains the discussion and concluding remarks.

2 Background

2.1 Single parameter estimation in quantum systems

A fundamental problem in quantum parameter estimation is the design of precise estimators of an unknown parameter $\theta \in \Theta$ characterizing a quantum state based on measurements of the system. In this context, a quantum system is modeled as a Hilbert space $\mathcal{H}$, and its state is described by a density operator ρ, which is a self-adjoint positive operator with unit trace on $\mathcal{H}$. The process of encoding the unknown parameters into a probe state ρ is accomplished by a dynamical process, which, when it can be represented as a unitary transformation $U(\theta)$, yields the state

$$\rho(\theta) = U(\theta)\rho U^\dagger(\theta), \quad \theta \in \Theta. \tag{1}$$

Estimation of θ can be achieved through an estimator that is a function that takes a sample of size N from a measurement of the quantum system as an input and produces an estimate of the unknown parameter. The most general description of a measurement process is a POVM [4]. Given a quantum system $\mathcal{H}$ and an outcome space $\mathcal{X} \subseteq \mathbb{R}^k$ for a measurement, a POVM is a map $M : \mathcal{B}(\mathcal{X}) \to B(\mathcal{H})$ from the set of events of our random experiment $\mathcal{B}(\mathcal{X})$ to the space of bounded operators on $\mathcal{H}$, denoted by $B(\mathcal{H})$, that satisfies the following conditions [4, 29, 30]:

i. $M(\emptyset) = 0, \quad M(\mathcal{X}) = I$

ii. $M(B) \geq 0, \quad \forall B \in \mathcal{B}(\mathcal{X})$

iii. For every family of mutually disjoint events $\{B_n\}_{n=1}^{\infty} \subset \mathcal{B}(\mathcal{X})$, so that $B_i \cap B_j = \emptyset \ \forall i \neq j$, that satisfies $\cup_{j=1}^{\infty} B_j = B \in \mathcal{B}(\mathcal{X})$, then $M(B) = \sum_{j=1}^{\infty} M(B_j)$.

In particular, when the state of the system is $\rho(\theta)$, the observed data $x \in \mathcal{X}$ of a measurement M is an outcome of a random variable $X \in \mathcal{X}$ distributed according to the density function $f(x \mid \theta; M)$ (or probability mass function in the case of discrete random variables) given by the Born's rule

$$f(x \mid \theta; M) = \mathrm{Tr}\left[M(x)\rho(\theta)\right]. \tag{2}$$

Thus, any sample from the application of a sequence of N POVMs $M_1, \ldots, M_N$ in a quantum system is represented as a sequence of N random variables $\vec{X}_N = X_1, \ldots, X_N$. It follows that any estimator $\widehat{\theta}\,(X_1, \ldots, X_N)$ based on this sample is also a random variable with expected value

$$\mathrm{E}_\theta\left[\widehat{\theta}(\vec{X}_N)\right] = \int_{\mathcal{X}^N} \widehat{\theta}(x_1, \ldots, x_N) f(x_1, \ldots, x_N \mid \theta; M_1, \ldots, M_N) dx_1 \cdots dx_N. \tag{3}$$

To find optimal estimators for all $\theta \in \Theta \subset \mathbb{R}$, the concept of unbiased estimator plays a crucial role. An estimator $\widehat{\theta}(\vec{X}_N)$ is unbiased if $\mathrm{E}_\theta\left[\widehat{\theta}(\vec{X}_N)\right] = \theta$ for all $\theta \in \Theta$ [31]. The performance of unbiased estimators is characterized by their variance, which is bounded by the Cramér-Rao bound [31]. This bound corresponds to the classical limit of precision for all unbiased estimators, and is given by the inverse of the Fisher information denoted by $F_X(\theta)$. Given a sample X produced by a POVM M, the Fisher information

$$F_X(\theta) = \int_{\mathcal{X}} f(x \mid \theta; M) \left[\frac{\partial}{\partial\theta} \log\left(f(x \mid \theta; M)\right)\right]^2 dx \tag{4}$$

quantifies the amount of information about the parameter θ that can be extracted from the sample X [28, 32]. The ultimate limit of precision, dictated by quantum mechanics, is achieved by optimizing $F_X(\theta)$ over all possible POVMs, resulting in the quantum Fisher information (QFI). Consequently, the variance of any unbiased estimator is lower bounded by the inverse of the QFI, referred to as the quantum Cramér-Rao bound (QCRB) [28, 32, 33]. The objective in quantum parameter estimation is to devise estimators and quantum measurement schemes that attain the QCRB for any value of the parameter $\theta \in \Theta$.

2.2 Optical phase estimation based on dyne-detection

A central task in optical quantum metrology is the estimation of an unknown phase $\theta \in [0, 2\pi)$ encoded in a photonic quantum state by the unitary process $U(\theta) = e^{-i\hat{n}\theta}$, where $\hat{n}$ is the photon number operator. The standard quantum state probe for optical phase estimation is the coherent state $|\alpha\rangle\langle\alpha|$, $\alpha \in \mathbb{C}$, in which photons exhibit classical correlations [13, 34]. For this quantum state, the QCRB for any unbiased estimator $\widehat{\theta}$ and N independent copies of the system is [4]

$$\mathrm{Var}[\widehat{\theta}] \geq \frac{1}{4N\mathrm{E}\left[\hat{n}\right]}, \tag{5}$$

This limit in precision defines the SNL (or the coherent state limit).

To surpass the SNL for optical phase estimation, it is necessary to employ states with quantum correlations, such as squeezed vacuum states. These states are defined by the density operator [13]:

$$\rho_r = |0, r\rangle\langle 0, r| = \hat{S}(r)\,|0\rangle\langle 0|\,\hat{S}^\dagger(r), \tag{6}$$

where $\hat{S}(r) = e^{\frac{1}{2}\left(re^{-i\gamma}\hat{a}^2 - re^{i\gamma}\hat{a}^\dagger\right)}$ is the squeezing operator, $r \in \mathbb{R}$, $\gamma \in [0, 2\pi)$, and $\hat{a}$ and $\hat{a}^\dagger$ are the annihilation and creation bosonic operators, respectively. Through the unitary transformation $U(\theta)$, the squeezed vacuum state in Eq. (6) results in the parameter-dependent state $\rho(\theta) = U^\dagger(\theta)\rho U(\theta)$. The corresponding QCRB for this state for any unbiased estimator $\widehat{\theta}$ and N independent copies of the system is given by [26]:

$$\mathrm{Var}[\widehat{\theta}] \geq \frac{1}{2N\sinh^2(2r)} = \frac{1}{8N\left(\mathrm{E}\left[\hat{n}\right]^2 + \mathrm{E}\left[\hat{n}\right]\right)}, \tag{7}$$

where r represents the squeezing strength of $\hat{S}(r)$ [35, 36]. This bound exhibits a superior scaling with $\mathrm{E}\left[\hat{n}\right]$ compared to the coherent state in Eq. (5). However, it is worth noting that due to the π-inversion symmetry inherent to squeezed vacuum states [37] (see Fig. 1-**i**), any estimation strategy based on these states is constrained to phases within the range of $[0, \pi)$.

The standard measurement approach for optical phase estimation is the heterodyne measurement [38, 39]. This measurement involves simultaneous sampling of two orthogonal components of the electromagnetic field within the complex plane, namely $\hat{X}_\phi$ and $\hat{X}_{\phi+\pi/2}$, by utilizing the quadrature decomposition of the input field [10]. Here, the quadrature operator $\hat{X}_\phi$ is defined as:

$$\hat{X}_\phi = \frac{\hat{a}^\dagger e^{i\phi} + \hat{a}e^{-i\phi}}{2}. \tag{8}$$

The POVM associated with the heterodyne measurement is described by coherent state projectors $M_{\mathrm{Het}} =$

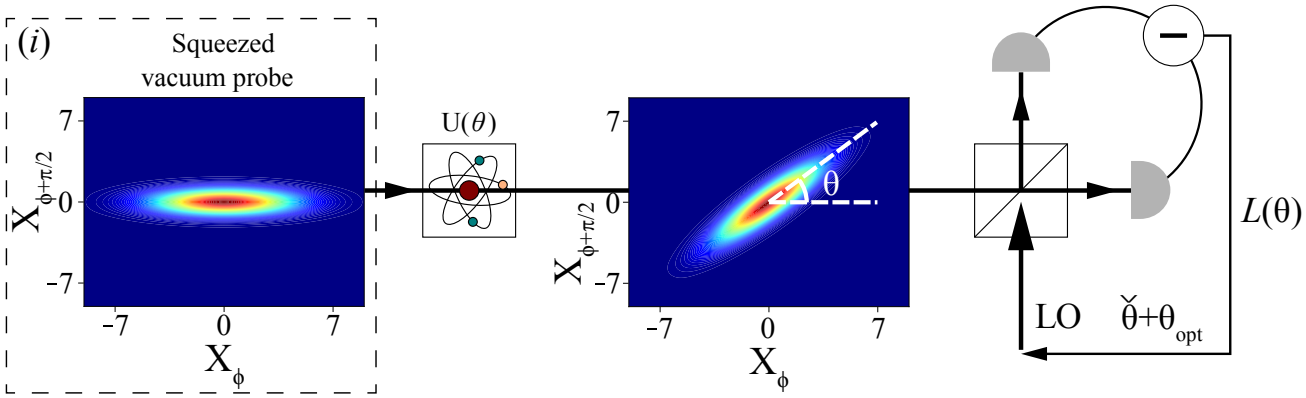

Figure 1: Adaptive estimation strategy for optical phase estimation with squeezed vacuum probe states $|0,r\rangle\langle 0,r|$. The strategy employs locally optimal POVMs, $M_{\check{\theta}}$ in Eq. (16) with $\check{\theta} \in [0,\pi/2)$, to produce a maximum likelihood estimate of θ, and updates the value $\check{\theta}$ for subsequent adaptive steps. The measurement process is iteratively repeated during the adaptive strategy. Inset **(***i***)** shows the Husimi Q representation for the initial squeezed vacuum state. Note that due to the internet symmetry properties of squeezed vacuum, these quantum probes can only encode the phase modulo π.

$\{\pi^{-1}|z\rangle\langle z| : z \in \mathbb{C}\}$, with outcomes corresponding to complex numbers, and with the corresponding Fisher information:

$$F_Z(\theta) = 4\sinh^2(r)\,. \tag{9}$$

The inverse of Eq. (9) is known as the heterodyne limit for the precision of any unbiased estimator $\widehat{\theta}$ for all $\theta \in [0,\pi)$ with squeezed vacuum states.

Going beyond estimation strategies based on heterodyne detection, homodyne detection can surpass the heterodyne limit for a suitable set of values of θ. Homodyne provides information about the quadrature $\hat{X}_\phi$ of the input signal using a local oscillator (LO) phase reference field and interference [10]. Specifically, in the limit of strong LO, Eq. (8) represents a self-adjoint operator with a spectral measure given by [38]:

$$\hat{X}_\phi = \int_{-\infty}^{\infty} x\Pi(dx), \tag{10}$$

where $\Pi(B) = 1_B(x)$ (or symbolically in Dirac notation, $\Pi(dx) = |x\rangle\langle x|\,dx$), for any $B \in \mathcal{B}(\mathbb{R})$. Consequently, the homodyne measurement can be described by the POVM $M_{\text{Hom}} = \{\Pi(dx)\}$, with the outcome space being the real numbers [40].

For squeezed vacuum state probes in Eq. (6), the outcomes $x \in \mathbb{R}$ of the homodyne measurement are distributed according to a normal random variable with probability density function

$$f(x \mid \theta) = \frac{1}{\sqrt{2\pi\sigma^2(\theta)}} \exp\left[-\frac{x^2}{2\sigma^2(\theta)}\right], \tag{11}$$

where θ denotes the unknown phase and

$$\sigma^2(\theta) = \left[e^{-2r}\cos^2(\theta) + e^{2r}\sin^2(\theta)\right] \tag{12}$$

denotes the variance. The Fisher information $F_X(\theta)$ for the homodyne measurement is then

$$F_X(\theta) = \frac{2\sinh^2(2r)\sin^2(2\theta)}{\left(\sigma^2(\theta)\right)^2}. \tag{13}$$

Notably, the classical Fisher information of the homodyne measurement coincides with the QFI when the squeezing strength r satisfies:

$$r = -\frac{1}{2}\log(\tan(\theta)), \tag{14}$$

or equivalently, when the parameter θ corresponds to the optimal value θ_{opt} given by

$$\theta_{\text{opt}} = \frac{\arccos\left(\tanh(2r)\right)}{2} \tag{15}$$

which tends to zero as r increases. Consequently, the homodyne measurement can surpass the heterodyne limit in the neighborhood of θ_{opt}. However, outside this neighborhood, estimators based on a sample $\vec{X}_N$ obtained from N independent and identical homodyne measurements cannot achieve this optimal level of precision (see Fig. 9).

To overcome this limitation, adaptive estimation protocols have been proposed. One such protocol [22, 25, 26], that we refer to as the two-step protocol, considers a reduced parameter space $[0,\pi/2)$, and utilizes homodyne detection and one subsequent adaptation of the probe state to surpass the heterodyne limit within this phase range. This strategy approaches the QCRB in the asymptotic limit for phases around the optimal phase θ_{opt} [22, 25]. However, far from this optimal phase, its performance significantly deviates from the QCRB. Moreover, when considering the full range of phases that can be encoded in squeezed vacuum probes $[0,\pi)$, this two-step estimation strategy is not expected to produce satisfactory results, due to the periodicity of the likelihood function from homodyne outcomes.

In a more general measurement setting, Gaussian [38, 41] and generalized dyne measurements [42, 43], which extend the concepts of homodyne and heterodyne, have a large potential for quantum metrology [41], sensing [44], and communications [45], and for studying the dynamical evolution of quantum systems under continuous measurements [42, 46]. Moreover, the combination of optimal control, quantum feedback, and Gaussian measurements allows for implementations of optimal phase measurements for single qubits, even across the full range of phases [47, 48]. However, optimal phase measurements based on quantum feedback and optimal control for quantum correlated states, such as squeezed states, are still unknown, but are expected to be highly complex in practice.

In this work, we propose an adaptive estimation strategy based on homodyne detection, that leverages the framework of AQSE, which, under certain regularity conditions (see Appendix: 8.1), yields a consistent and efficient estimator for any phase $\theta \in [0, \pi/2)$. A key element of this approach is to use samples that lead concave likelihood functions, ensuring the asymptotic normality of the Maximum Likelihood Estimator (MLE) [27, 28]. This property guarantees the asymptotic saturation of the QCRB in Eq. (7) for any $\theta \in [0, \pi/2)$. We further generalize this adaptive strategy to incorporate heterodyne measurements enabling phase estimation within $[0, \pi)$, while maintaining a quantum-optimal performance in the asymptotic limit.

3 Optimal adaptive homodyne phase estimation

In practice, it is generally impossible to find a POVM and an unbiased estimator capable of saturating the QCRB for all $\theta \in \Theta$. However, it is often possible to find a POVM and an unbiased estimator that can achieve this bound for a specific value of the parameter within a neighborhood around a point $\theta_0 \in \Theta$. These types of POVMs are referred to as locally optimal at θ_0. Moreover, if it is possible to construct a collection of such locally optimal POVMs for any $\theta \in \Theta$ while satisfying a set of regularity conditions pertaining to the probability distributions of their outcomes (see Appendix: 8.1), then it is possible to use an adaptive estimation method, known as AQSE [27], capable of saturating the QCRB in the asymptotic limit for the MLE $\forall \theta \in \Theta$.

Building upon this understanding, the proposed adaptive phase estimation strategy with squeezed vacuum states is constructed based on two elements. The first element involves the construction of a set of POVMs through homodyne measurements that are locally optimal for any value of the parameter, that is the optical phase θ within the range $\theta \in [0, \pi/2) = \Theta$. The second element is the construction of an estimator that achieves the QCRB for any given value of the phase θ, while also being locally unbiased at the true phase $\theta_0 \in \Theta$ [4, 27].

To construct the set of locally optimal POVMs, we refer to Eq. (15), which shows that the homodyne POVM $M_{\text{Hom}} = \{\Pi(dx)\}_{x\in\mathbb{R}}$ in Eq. (10) is locally optimal at θ_{opt}. This is because the samples obtained from M_{Hom} have a Fisher information equal to the QFI at this specific phase. Furthermore, given the asymptotic unbiasedness of the MLE, and its subsequent local unbiasedness, the estimator effectively saturates the QCRB (Eq. (7)) in the asymptotic limit at θ_{opt}. Consequently, by appropriately incorporating a phase shift into the elements of M_{Hom}, it is possible to construct a set of locally optimal POVMs for any phase $\theta \in [0, \pi/2)$.

To this end, we introduce a phase shift $U\left(\check{\theta} - \theta_{\text{opt}}\right)$, which allows us to define a new set of POVMs for each $\check{\theta} \in [0, \pi/2)$ as follows:

$$M_{\check{\theta}}(dx) = \left\{U\left(\check{\theta} - \theta_{\text{opt}}\right)\Pi(dx)U^{\dagger}\left(\check{\theta} - \theta_{\text{opt}}\right)\right\}. \tag{16}$$

Here $M_{\check{\theta}}(dx)$ denotes the POVM elements obtained by applying the phase shift to the original POVM elements $\Pi(dx)$ of M_{Hom}. Note that the phase distribution of $M_{\check{\theta}}(dx)$ over the state $\rho(\theta)$ becomes:

$$\begin{aligned} f(x \mid \theta; M_{\check{\theta}}) &= \text{Tr}\left[U\left(\check{\theta} - \theta_{\text{opt}}\right)|x\rangle\langle x|U^{\dagger}\left(\check{\theta} - \theta_{\text{opt}}\right)\rho(\theta)\right] \\ &= f(x \mid \theta + \theta_{\text{opt}} - \check{\theta}; M_{\text{Hom}}). \end{aligned} \tag{17}$$

Evaluated at $\check{\theta} = \theta$, this distribution is the same as the distribution for the outcomes of the POVM M_{Hom} at θ_{opt}, which shows that the POVM $M_{\check{\theta}}(dx)$ is locally optimal at θ. From this observation and based on the AQSE framework, then it is possible to construct a multi-step estimation strategy based on adaptive homodyne measurements, which provide a set of locally optimal measurements, for which the distribution of the sequence of estimators converges to a normal distribution with variance equal to the inverse of the QFI (see Appendix 8.2).

Figure 1 shows the concept of the proposed phase estimation strategy based on adaptive homodyne measurements. For a set of N input squeezed probe states $\{|0, r\rangle\langle 0, r|\}$, a phaseshift $U(\theta)$ encodes the parameter θ in the probes. The adaptive strategy then implements the POVM $M_{\check{\theta}_1}$ with an initial (random) guess $\check{\theta}_1 \in [0, \pi/2)$ over $\nu = N/m$ of these states, yielding a measurement sample $\vec{X}_\nu(\check{\theta}_1) = X_1(\check{\theta}_1), \ldots, X_\nu(\check{\theta}_1)$. The MLE applied to $\vec{X}_\nu(\check{\theta}_1)$, $\widehat{\theta}_{\text{MLE}}\left(\vec{X}_\nu(\check{\theta}_1)\right)$, results in an estimate $\check{\theta}_2 = \widehat{\theta}_{\text{MLE}}\left(\vec{x}_\nu(\check{\theta}_1),\right)$ of θ for the firt adaptive step. This estimate $\check{\theta}_2$ then becomes the best guess for the subsequent adaptive step, and the process is repeated m times iteratively during the strategy.

3.1 Estimator

A key aspect of the parameter estimation strategy is the selection of an estimator that allows for the saturation of the QCRB. We identify the necessary conditions to ensure the asymptotic consistency and normality of the MLE and the saturation of the QCRB through the adaptive strategy for any $\theta \in [0, \pi/2)$. Assuming that the Fisher information is different from zero for any θ [1], the MLE saturates the QCRB given that:

(a) the MLE is a single-valued function;

(b) the MLE is obtained as a stationary point of the likelihood function; and

(c) the derivatives of the likelihood function at θ exist up to a high-enough order so that they can be effectively approximated using a Taylor series [27, 49].

We observe that (a) is automatically satisfied, since the measurement outcomes from the proposed strategy follow a normal distribution, as shown Eq. (11). This condition ensures the sufficient smoothness of the likelihood function for any $\theta \in [0, \pi/2)$ in each adaptive step. Moreover, by restricting the parameter space to the interval $[0, \pi/2)$, this condition guarantees the uniqueness of the MLE for any $\theta \in [0, \pi/2)$. Thus, the remaining task is to determine the conditions under which the MLE corresponds to a stationary point of the likelihood function, leading to its asymptotic normality. To this end, we first analyze the MLE for a sample from the first adaptive step.

Given a sample $\vec{X}_\nu(\check{\theta}_1) = (X_1, X_2, \ldots, X_\nu)$ of size ν from the POVM $M_{\check{\theta}_1}$ at the first adaptive step, and evaluating the likelihood from Eq. (11) at $\theta_* = \left(\theta + \theta_{\text{opt}} - \check{\theta}_1\right)$ modulo $\pi/2$, we obtain the MLE for θ as:

$$\widehat{\theta}_{\text{MLE}}(\vec{X}_\nu) = \arccos\left[\frac{e^r\sqrt{e^{2r} - \frac{1}{\nu}\sum_{i=1}^{\nu} X_i^2}}{\sqrt{e^{4r}-1}}\right] - \theta_{\text{opt}} + \check{\theta}_1. \tag{18}$$

The set of homodyne outcomes for which $e^{2r} - \frac{1}{\nu}\sum_{i=1}^{\nu} X_i^2 > 0$ in Eq. (18), which results in a real-valued $\widehat{\theta}_{\text{MLE}}(\vec{X}_\nu)$, yields a MLE corresponding to a stationary point of the likelihood within $[0, \pi/2)$. Therefore, the probability of obtaining a non-real solution of Eq. (18) at $\check{\theta}_1 = \theta_{\text{opt}}$ is:

$$\begin{aligned} P\left(e^{2r} < \frac{1}{\nu}\sum_{i=1}^{\nu} X_i^2 \mid \check{\theta}_1 = \theta_{\text{opt}}\right) &= P\left(\sum_{i=1}^{\nu}\frac{X_i^2}{\sigma^2(\theta)} > e^{2r}\left(\frac{\nu}{\sigma^2(\theta)}\right)\right) \\ &= 1 - P\left(\sum_{i=1}^{\nu}\frac{X_i^2}{\sigma^2(\theta)} \leq e^{2r}\left(\frac{\nu}{\sigma^2(\theta)}\right)\right) \\ &= 1 - P_{SP}(\theta). \end{aligned} \tag{19}$$

Here, $P_{SP}(\theta)$ is the probability that the likelihood function has its global maximum at a stationary point at θ. We note that $Q = \sum_{i=1}^{\nu}\frac{X_i^2}{\sigma^2(\theta)}$ is the sum of squares of ν independent standard normal random variables and follows a chi-squared distribution with ν degrees of freedom ($Q \sim \chi^2(\nu)$) [31].

Figure 2 shows the probability of obtaining a non-real solution of Eq. (18) as a function of θ for different values of the squeezing strength r and sample size ν. We observe that as θ deviates from the optimal value θ_{opt} in Eq. (15), the probability that the estimates were not obtained from a stationary point in the likelihood function within the interval $[0, \pi/2)$ becomes different than zero. We also note that the region in which the global maximum of the likelihood is not reached at a stationary point decreases as we increase the degrees of freedom ν (sample size in the adaptive step) or the squeezing strength r. Moreover, when $e^{2r} - 1/\nu\sum_{i=1}^{\nu} X_i^2 < 0$ (regions where the global maximum does not correspond to a stationary point) the MLE in Eq. (18) corresponds to the boundary point $\pi/2$. This event introduces a bias in the estimate for subsequent adaptive steps, leading to a decrease in the precision of the final estimate. This effect in the estimate becomes more detrimental when the phase to be estimated θ_0 is close to the boundary point $\pi/2$ (see Figure 2) as can be observed in the previous two-steps protocols [22]. We can attribute this issue to the Fisher information being zero at $\theta = \pi/2$ (or $\theta = 0$). As a result, the information that can be obtained about the phase at these boundary points vanishes.

The proposed strategy address this problem by first making a random guess $\check{\theta}_1 \in [0, \pi/2)$ in the first adaptive step. This initial random guess reduces in average the probability that the MLE does not arise from a stationary point within $[0, \pi/2)$ in Eq. (19). According to the law of total probability

[1] This assumption holds except in the first adaptive step if $\check{\theta}_1 = \theta + \theta_{\text{opt}}$. However, in our adaptive strategy, $\check{\theta}_1$ is chosen at random within $[0, \pi/2)$. Therefore the probability of observing this event is zero.

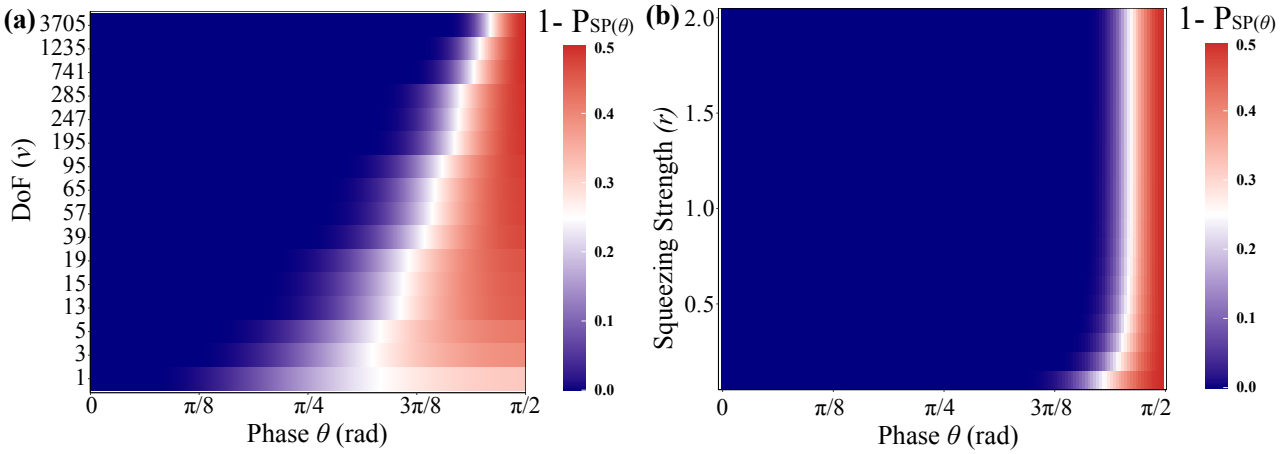

Figure 2: Probability that the likelihood function does not have its global maximum at a stationary point $1 - P_{SP}(\theta)$ within $[0, \pi/2)$ from Eq. (19). **(a)** Probability $1-P_{SP}(\theta)$ for different degrees of freedom (DoF) ν (number of probes in each adaptive step) with $r = 1$. **(b)** Probability $1 - P_{SP}(\theta)$ for different values of squeezing strength r with $\nu = 3705$. By ensuring that the global maximum of the likelihood function is attained at a stationary point within the interval $[0, \pi/2)$, we mitigate the bias introduced by boundary estimates and enhance the performance of the adaptive estimation process (See main text for details).

$$
\begin{aligned}
P\left(e^{2r} < \frac{1}{\nu}\sum_{i=1}^{\nu} X_i^2\right) &= \mathrm{E}_{\hat{\theta}_0}\left[P\left(e^{2r} < \frac{1}{\nu}\sum_{i=1}^{\nu} X_i^2 \mid \check{\theta}_1\right)\right] \\
&= \int_0^{\pi/2} d\check{\theta}_1 P\left(\sum_{i=1}^{\nu}\frac{X_i^2}{\sigma^2(\theta_*)} > e^{2r}\left(\frac{\nu}{\sigma^2(\theta_*)}\right)\right) \\
&= \int_0^{\pi/2} d\check{\theta}_1 P_{SP}(\theta_*).
\end{aligned}
\tag{20}
$$

Moreover, this probability decreases as the sample size ν increases, as shown in Fig. 3. As a final step, to guarantee that the MLE always arises from stationary points, we introduce a modified estimator

$$
\widehat{\theta}^{\mathrm{U}}_{\mathrm{MLE}}(\vec{X}_\nu) = \begin{cases} \widehat{\theta}_{\mathrm{MLE}}(\vec{X}_\nu) & \text{if } e^{2r} - 1/\nu\sum_{i=1}^{\nu} X_i^2 \geq 0, \\ \widehat{\theta}_{\mathrm{MLE}}(\vec{X}_s) & \text{otherwise,} \end{cases} \tag{21}
$$

where $\vec{X}_s$ is a subsequence of $\vec{X}_\nu$ constructed by iteratively removing the highest values of $\vec{X}_\nu$ in descending order until the condition $e^{2r} - 1/s\sum_{i=1}^{s} X_i^2 \geq 0$ is satisfied. We note that while the estimator ignores a few measurement outcomes from the sample, the probability of this event happening is low, and this modified estimator greatly improves the final variance of the estimates. Moreover, it is worth noting that the modified estimator in Eq. (21) is only necessary in the first adaptive step. Once an estimate $\check{\theta}$ sufficiently close to the true value θ is obtained, the subsequent adaptive steps will result in samples close to θ_{opt}. Therefore, for sufficiently large values of r, and moderate ν, this procedure makes the probability in Eq. (19) tend to zero, guaranteeing the asymptotic efficiency of the MLE from the adaptive strategy.

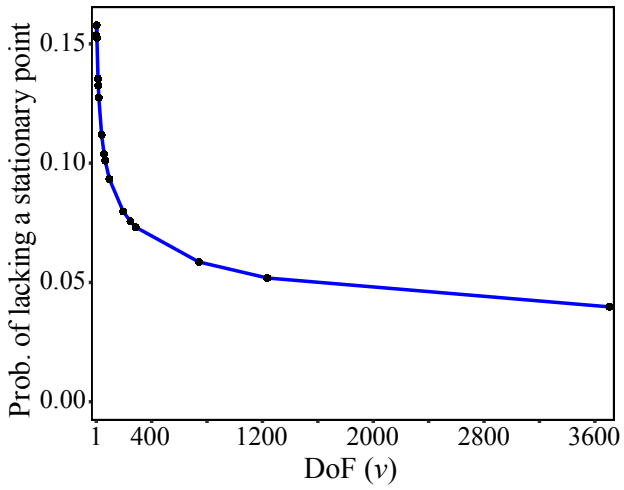

Figure 3: Conditional probability (Eq. (20)) that the likelihood function does not have its global maximum at a stationary point within $[0, \pi/2)$, given $\check{\theta}_1$ uniformly distributed from 0 to $\pi/2$. The black points show numerical evaluations of (Eq. (20)) for several ν, and the blue line is a guide for the eye showing the trend as a function of ν. This probability is upper bounded for $\nu = 1$, and decreases as ν increases. The parameter ν corresponds to the degrees of freedom (DoF) for $Q = \sum_{i=1}^{\nu} \frac{X_i^2}{\sigma^2(\theta)}$, which follows a chi-square distribution.

3.2 Proof of optimality of the adaptive estimation strategy

Appendix 8.2 gives a mathematical proof of the optimality of the proposed estimation strategy based on adaptive homodyne detection. The proof first establishes that by satisfying the regularity conditions outlined in Appendix 8.1, the probability of obtaining an estimate far from the true value θ_0 decreases exponentially to zero as the number of adaptive steps increases. This result demonstrates the *almost sure convergence* of the MLE to θ_0 (asymptotic consistency) [31]. Subsequently, using the asymptotic consistency of the estimator, we prove that the limiting distribution of the MLE, as the number of adaptive steps tends to infinity, is a normal distribution with mean θ_0 and variance equal to the inverse of the QFI (asymptotic normality). This demonstrates the convergence of the proposed adaptive strategy to the QCRB.

4 Performance of the adaptive strategy

We evaluate the performance of the adaptive estimation strategy based on locally optimal POVMs, Eq. (16), with the modified estimator in Eq. (21). We conduct Monte Carlo simulations varying the sample size ν, number of adaptive steps m, and squeezing strength r. We investigate the precision and efficiency of the estimation strategy and its convergence towards the QCRB in Eq. (7) for $\theta \in [0, \pi/2)$. Considering that the estimator $\widehat{\theta}\left(\vec{X}_\nu(\check{\theta}_1), \ldots, \vec{X}_\nu(\check{\theta}_m)\right)$ has a periodic distribution with period $\pi/2$, we evaluate the precision of $\widehat{\theta}\left(\vec{X}_\nu(\check{\theta}_1), \ldots, \vec{X}_\nu(\check{\theta}_m)\right)$ by using the corresponding Holevo variance [4, 50]:

$$\mathrm{Var}_\theta\left[\widehat{\theta}\left(\vec{X}_\nu(\check{\theta}_1), \ldots, \vec{X}_\nu(\check{\theta}_m)\right)\right] = \frac{\left[\mathrm{E}\left[\cos\left(\frac{2\pi}{P}\left(\widehat{\theta}\left(\vec{X}_\nu(\check{\theta}_1), \ldots, \vec{X}_\nu(\check{\theta}_m)\right) - \theta\right)\right)\right]\right]^{-2} - 1}{\left(\frac{2\pi}{P}\right)^2}, \tag{22}$$

where the factor P represents the period of the estimator's distribution, in our case $P = \pi/2$.

Figure 4 shows the results for the Holevo variance for $\widehat{\theta}\left(\vec{X}_\nu(\check{\theta}_1), \ldots, \vec{X}_\nu(\check{\theta}_m)\right)$ within $\theta \in [0, \pi/2)$ for adaptive estimation strategies based on homodyne detection and squeezed vacuum for different numbers of adaptive steps m from 3 to 15. For all these cases, we consider a strategy with a total number of copies of the probe state $N = 3705$ with squeezing strength $r = 1.01$, so that each adaptive step contains $\nu = N/m$ probe states (These parameters were chosen for easy comparison with previous works). The results shown in Figure 4 are obtained from the average of five Monte Carlo simulations, each with 1×10^4 runs of the strategy. The homodyne measurement without feedback and the two-step adaptive homodyne strategy from Ref. [22] are shown for comparison. All the results have been normalized to the QCRB $= QFI^{-1}$. For these simulations, sampling process employed the method of rejection sampling [51], while the optimization employed the method of generalized simulated annealing over the interval $[0, \pi/2]$ [52].

We observe that the proposed multi-step adaptive estimation strategy based on homodyne detection consistently outperforms the non-adaptive and the two-step homodyne strategies [22]. Moreover, as can be observed in Figure 4 (a) and the zoom in Figure 4 (b), this adaptive homodyne strategy progressively approaches the QCRB (dashed horizontal line), and is expected to saturate this bound for all values of $\theta \in [0, \pi/2)$ in the limit of many adaptive steps. For instance, the proposed adaptive estimation strategy with $m = 15$ adaptive steps achieves a precision of just 7% above the QCRB for phases $\theta \in [0, \pi/2)$ on average, compared to 42% with two steps [22]. We further note that while the two-step strategy in [22] shows a smaller variance for $\theta \approx \theta_{\text{opt}}$ compared to the proposed strategy with small $m = 3, 5$, its performance far from θ_{opt} deviates significantly from the QCRB, as can be seen in Figure 4 (b) (see also Appendix 8.3). Moreover, as discussed in the proof in Appendix 8.2, by construction the proposed strategy ensures an asymptotic quantum-limited performance. These results highlight the fundamental advantage of this multi-step adaptive strategy for parameter estimation, and underscore its potential for optical phase estimation and quantum metrology.

5 Loss and Noise Effects

5.1 Losses

The performance of the adaptive estimation strategy for optical phase estimation becomes sub-optimal in the presence of channel noise and loss, and when the detectors have reduced quantum efficiency. Most of these effects can be modeled as a mixing of the input probe with the vacuum state in a beam splitter. This mixing process adds thermal photons to the probe incident into the homodyne detector, depending on the transmission T of the beam splitter [35, 53]. Moreover, imperfect quantum efficiency of the detectors can be modeled as a lossy channel, which further contributes with additional thermal photons proportional

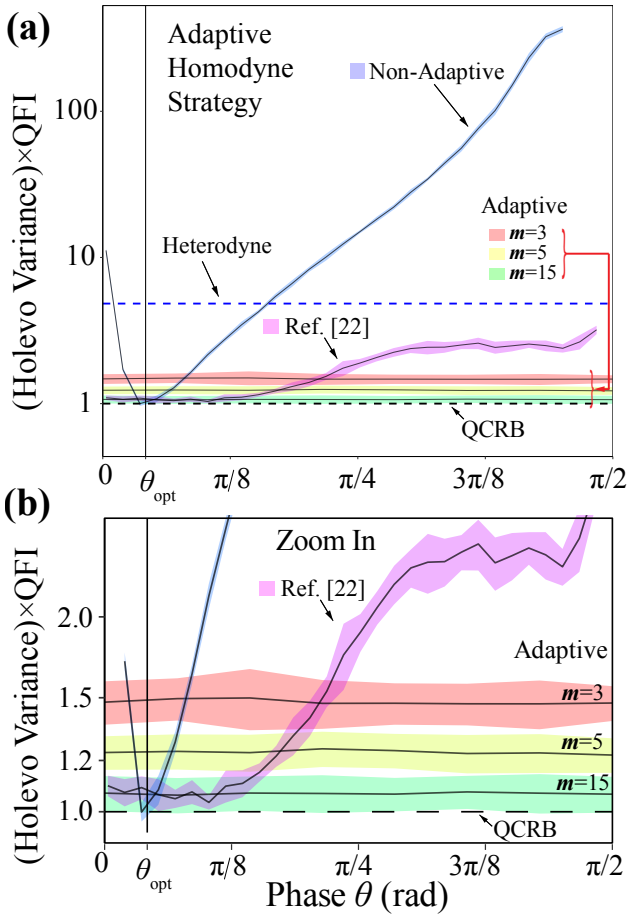

Figure 4: **(a)** Holevo variance of the adaptive estimation strategy based on the AQSE formalism as a function of θ, for different numbers of adaptive steps m, with $N = 3705$ total independent copies of the probe state with squeezing strength of $r = 1.01$. The y-axis shows the Holevo variance in logarithmic scale normalized to the inverse of the QFI in Eq. (7), corresponding to the QCRB. The magenta line shows the two-step adaptive estimation scheme from Ref. [22], and the blue curve shows the estimation with homodyne detection without feedback. The shaded regions represent a one standard deviation. **(b)** Zoom in the region close to the QCRB.

to T [35, 38, 54]. Specifically, the lossy channel modeled as a beam splitter with transmittance $0 < T < 1$ maps the squeezed vacuum state $\rho_r = |r,0\rangle\langle 0,r|$ into a squeezed thermal state

$$\rho_{\beta,r_l} = S(r_l)\left[(1-\mathrm{e}^{-\beta})\sum_{n=0}^{\infty}\mathrm{e}^{-\beta n}|n\rangle\langle n|\right]S^{\dagger}(r_l), \tag{23}$$

where $r_l < r$. This transformation reduces the QFI compared to that squeezed vacuum states ρ_{r_l} [35, 53, 55] as:

$$F_Q^{\mathrm{Lossy}} = \left[\frac{T^2}{1+2T(1-T)\sinh^2(r)}\right]F_Q. \tag{24}$$

where $F_Q = 2\sinh^2(2r)$ is the QFI about θ for squeezed vacuum states with strength r. Therefore, the effect of linear losses on the QCRB can be effectively accounted for by an appropriate rescaling [35].

The squeezed thermal states resulting from losses further reduce the maximum classical Fisher information for the homodyne measurement [35]:

$$F_X^{\mathrm{Lossy}}(\theta_{\mathrm{opt}}) = \left[\frac{T^2}{1+4T(1-T)\sinh^2(r)}\right]F_Q. \tag{25}$$

Here, we have used the fact that the maximum of the Fisher information $F_X^{\mathrm{Lossy}}(\theta)$ is achieved at the optimal phase θ_{opt} in Eq (15), now for r_l.

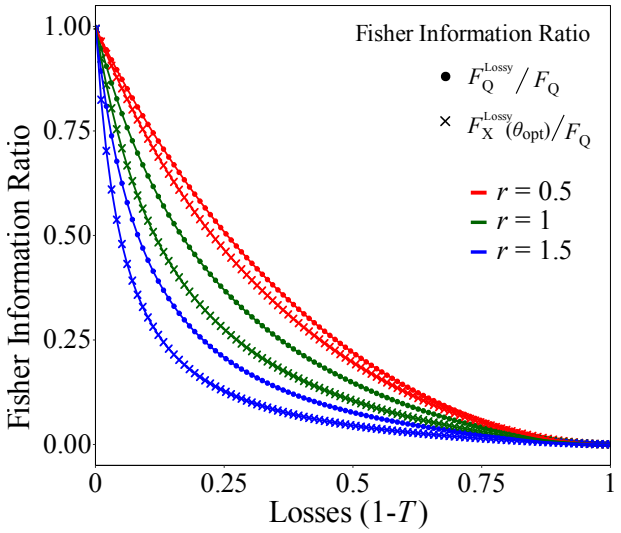

Figure 5: Fisher information ratios F_Q^{Lossy}/F_Q (dots) and $F_X^{\mathrm{Lossy}}(\theta_{\mathrm{opt}})/F_Q$ (crosses) for squeezed vacuum states as function of T for squeezing strength r of 0.5, 1.0 and 1.5.

Figure 5 shows the ratios F_Q^{Lossy}/F_Q (dots) and $F_X^{\mathrm{Lossy}}(\theta_{\mathrm{opt}})/F_Q$ (crosses) as a function of the losses $(1-T)$ and different values of r. We observe that probe states with larger r, are more sensitive to losses, showing a faster reduction in Fisher information with channel loss. Figure 5 also shows that the Fisher information F_Q^{Lossy} and $F_X^{\mathrm{Lossy}}(\theta_{\mathrm{opt}})$ approach F_Q only at $T \approx 1$. We note that losses $(T < 1)$ reduce the homodyne maximum Fisher information $F_X^{\mathrm{Lossy}}(\theta_{\mathrm{opt}}) < F_Q^{\mathrm{Lossy}}$, as seen in Eq. (25), which prevents the saturation of the QCRB solely with homodyne. Moreover, we note that in general the saturation of the QCRB for squeezed thermal states requires the implementation of non-Gaussian measurements [41]. However, devising non-Gaussian measurements that approach the QFI for this problem are highly complex, and their implementation is still an open problem [41].

In a more general setting, the problem of quantum channel estimation involves finding the optimal probe states and measurements to maximize information in a lossy and noisy channel [56, 57]. Recent advances in quantum channel estimation have found optimal probes for: Gaussian unitary channels (which consist of rotated squeezed states) [58], bosonic dephas-

ing channels [59], and complete positive trace preserving (CPTP) maps for qubits [57]. Moreover, in principle, it is possible to find the optimal quantum probe states for a general channel estimation problem using techniques of convex optimization including semidefinite and linear programming, and conic programming [57, 60, 61]. Here, we focus our discussion on squeezed probe states, and adaptive homodyne/heterodyne measurements, which are readily available in laboratory settings, and consider common sources of noise and imperfections, including linear losses.

5.2 Imperfect state preparation

The processes of state preparation in realistic implementations is often affected by small random errors yielding state preparation errors. Due to the Central Limit Theorem, the cumulative effect of small, independent errors in many probe states will tend to a normal distribution. Therefore, it is reasonable to assume that, under some state preparation errors, the squeezing strength r of the probe state $\rho_r = |r,0\rangle\langle 0,r|$ is the output of a random variable R with a normal distribution $\mathcal{N}\left(r_0, \sigma_r^2\right)$, where $\sigma_r^2 \geq 0$ is a small number relative to r_0.

To take into account state preparation errors of this kind in the adaptive strategy, we consider that the samples at every adaptive step are drawn from the conditional random variable $X \mid R$, where X is a sample from a homodyne measurement. We then analyze the strategy as described in Section 3 but considering state preparation errors. In this case, and without loss of generality by taking X as a sample of M_{Hom}, the Fisher information about θ contained in the conditional random variable $X \mid R$ is calculated with respect to the conditional density of X given R, that is,

$$F_{X|R}(\theta) = \mathrm{E}\left[F_{X|R=r}(\theta)\right], \tag{26}$$

where $F_{X|R=r}(\theta)$ corresponds to Eq. (13) at a specific value $R = r$. Therefore, in the asymptotic limit, the adaptive homodyne strategy samples around the phase that maximizes Eq. (26). In experimental settings, typically the range for σ_r lies between 0.01 and 0.02 [22, 62]. For state preparation errors with small variances σ_r^2, the optimal phase $\theta_{\text{opt}}^{noise}$ deviates slightly from the noiseless case θ_{opt}, and modifies the Fisher information.

Figure 6 shows $F_{X|R}(\theta)$ for standard deviations of r in state preparation $\sigma_r = 0.01$ and $\sigma_r = 0.02$ as a function of $\theta \in [0, \pi/2)$. We observe that errors in state preparation with σ_r of 0.01 and 0.02 have a negligible effect in the performance of the adaptive strategy, which shows a Fisher information around the QFI at the optimal phase θ_{opt}. We also note that since the QFI for squeezed vacuum is a nonlinear function of the squeezing strength r, the contribution of positive deviations of r from the mean r_0 to the expected value of $F_{X|R}(\theta)$ in Eq. (26) increases with r. This nonlinear effect causes the maximum of $F_{X|R}(\theta)$ to slightly surpass $F_{X|R=r}(\theta_{\text{opt}})$ corresponding to the QFI (dashed red line), as can be observed in the inset (i) of Figure 6.

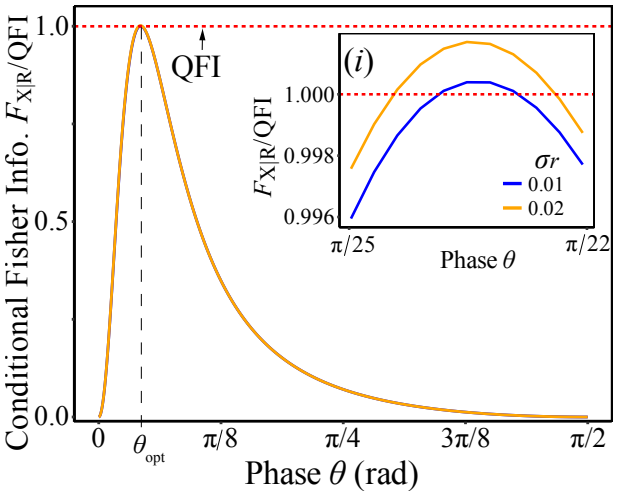

Figure 6: Expected Fisher information as function of θ with state preparation errors with normally varying squeezing strength for $r_0 = 1$ with σ_r of 0.01 and 0.02. The dashed red line corresponds to the QFI for squeezed vacuum states at $r = 1$. Inset (i) shows a zoom in the maximum of the curve showing the overshot effect due to the nonlinear dependence of $F_{X|R}(\theta)$ with r.

5.3 Phase errors in the homodyne local oscillator (LO)

As a case of study for measurement errors, we consider that the LO in the homodyne measurement is subject to small phase errors. Thus, the parameter $\check{\theta}$, describing the phase estimate and the setting for the POVM $M_{\check{\theta}}$ in the adaptive measurement protocol, can be considered as the output of a random variable $\check{\Theta}_{\text{lo}}$ with a normal distribution $\mathcal{N}\left(\check{\theta}_{\text{lo}}, \sigma^2(\check{\theta}_{\text{lo}})\right)$, centered at the ideal measurement setting $\check{\theta}_{\text{lo}}$ and with a variance $\sigma^2(\check{\theta}_{\text{lo}})$. Assuming that $\check{\theta}_{\text{lo}} \approx \theta$, we can evaluate the loss of information caused by these kinds of measurement errors by calculating the conditional Fisher information with respect to the random variable $X \mid \check{\Theta}_{\text{lo}}$,

$$F_{X|\check{\Theta}_{\text{lo}}} = \mathrm{E}\left[F_{X|\check{\Theta}_{\text{lo}}=\check{\theta}}\right], \tag{27}$$

where X is a sample from the POVM $M_{\check{\theta}}$ applied to the state $\rho_r = |r,0\rangle\langle 0,r|$.

Figure 7 shows Eq (27) as a function of the standard deviations $\sigma(\check{\theta}_{\text{lo}})$ in measurement implementation, ranging from 0.01 to 0.1 radians. We observe that errors in the phase reference for the homodyne detection has a moderate detrimental effect in the Fisher information, which decreases approximately to

half of the QFI for large LO phase noise of $\sigma(\check{\theta}_{\rm lo}) \approx 0.15$ rad. However, we note that this technical problem can be overcome by standard phase stabilization techniques [63, 64].

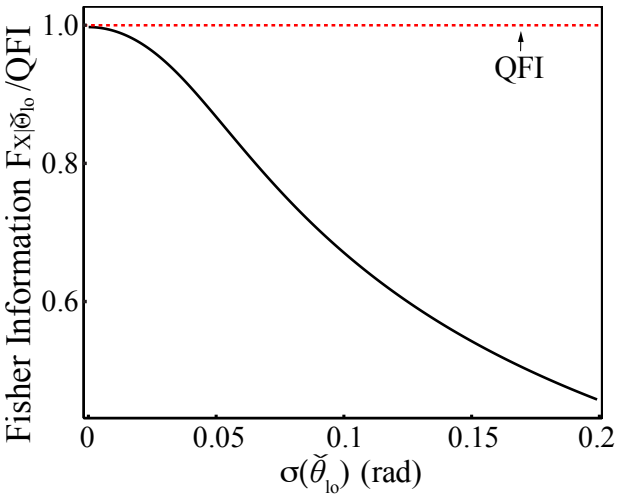

Figure 7: Expected Fisher information of the homodyne measurement as a function of $\sigma(\check{\theta}_{\rm lo})$ quantifying the phase errors in the LO for input states with a squeezing strength of $r = 1$ and measurement errors normally distributed around $\check{\theta}_{\rm lo} = \theta$. The dashed red line corresponds to the QFI for squeezed vacuum states at $r = 1$.

6 Combined homodyne-heterodyne (CHH) measurement strategy

In general, the problem of phase estimation involves estimation over the complete range of possible phases from 0 to 2π. However, when using squeezed vacuum states for phase estimation beyond the SNL, there is a physical limitation on the range of phases that can be estimated. Squeezed vacuum states are invariant under phase shifts of π, restricting the estimable phases to the interval $[0, \pi)$, which is half of the complete range in the general problem of phase estimation. This symmetry can be seen in the Husimi Q representation of the state ρ_r, $Q(\alpha) = \frac{1}{\pi} \langle \alpha | \rho_r | \alpha \rangle$ (see inset (i) Fig. 1), which shows that the squeezed vacuum probe can only encode the phase modulo π. Moreover, the measurement employed for decoding the phase can impose severe constraints on the range of phases that can be estimated. For instance, homodyne measurements further reduce the range of phases within which phase estimation is possible to $[0, \pi/2)$. This is because the probability distributions of outcomes from homodyne measurements in Eq. (11), associated with POVMs in Eq. (16), are $\pi/2$ periodic. Consequently, any strategy based on adaptive homodyne is restricted to estimating phases within the range $[0, \pi/2)$. To go beyond this limited range and enable phase estimation with squeezed vacuum over the entire range of phases $[0, \pi)$, it is necessary to include measurements beyond homodyne.

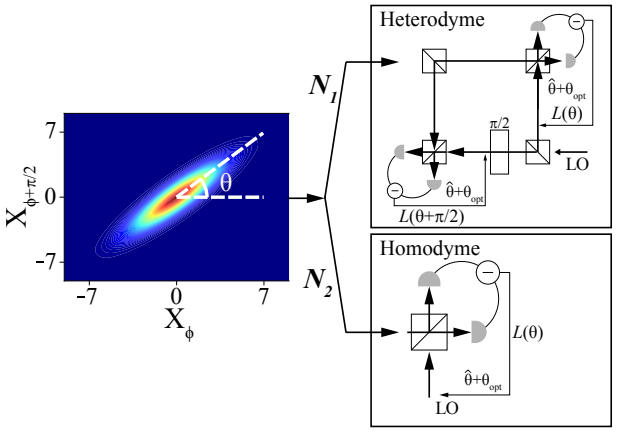

Figure 8: Combined homodyne-heterodyne (CHH) measurement strategy for phase estimation based on squeezed vacuum probes for phases $\theta \in [0, \pi)$. This strategy takes advantage of the capability of heterodyne measurements to unambiguously estimate phases within the whole parametric space $[0, \pi)$ for squeezed vacuum, overcoming the non-identifiability problem in the likelihoods from homodyne measurements. By employing a small sample of heterodyne measurements, the unknown phase θ is localized within a neighborhood within $[0, \pi)$. Then, the strategy employs adaptive homodyne for phase estimation within this neighborhood.

We propose a combined homodyne-heterodyne (CHH) measurement strategy that uses heterodyne to identify the neighborhood of the unknown phase within $[0, \pi)$, and subsequently, adaptive homodyne to implement an asymptotically optimal measurement strategy. This CHH measurement uses time sharing between heterodyne and homodyne, which is a special case of the generalized dyne measurement [41], and enables optimal phase estimation within $[0, \pi)$ in the asymptotic limit.

Figure 8 shows the schematic of the proposed CHH strategy. The strategy implements a heterodyne measurement on a small sample of N_1 probe states, denoted as $\vec{X}^{\rm Het}_{N_1}$, to determine the neighborhood in the parametric space $[0, \pi)$ to which the unknown phase belongs. This makes the parameter identifiable within $[0, \pi)$ solving the non-identifiability problem of homodyne [3], and produces a likelihood peaked around the true value. After the heterodyne sampling $\vec{X}^{\rm Het}_{N_1}$, the CHH strategy implements the adaptive homodyne strategy described in Section 3, with N_2 copies of the probe state and m adaptive measurements. By construction, when $N_2, m \to \infty$ (in the asymptotic limit), and N_1 is large enough such that the MLE from the heterodyne sampling $\widehat{\theta}\left(\vec{X}^{\rm Het}_{N_1}\right) \in [0, \pi/2)$ with high probability, this strategy saturates the QCRB Eq. (7) [3, 65] (see Appendix 8.4 for discussion of the proof). Thus, in the asymptotic limit this strategy is expected to be able to extract all the information about the phase encoded in the quantum probe and approach

the QCRB for any phase within $[0, \pi)$.

Figure 9 (a) shows the performance of the CHH phase estimation strategy enabling near quantum-optimal phase estimation for phases within $[0, \pi)$ with a finite number of samples. These results are obtained from the average of five Monte Carlo simulations considering $N = 3705$ copies of the squeezed vacuum probes with $m = 15$ adaptive steps, each with a sample of size $\nu = 247$. In this combined strategy, the first step consists of a heterodyne measurement with a sample of size $N_1 = \nu_1 = 247$. This sample is large enough to produce estimates with high probability in $[0, \pi/2)$, and it is significantly smaller than the total of subsequent (homodyne) samples $N_2 = \sum_{i=2}^{14} \nu_i = 3458$. We note that within the statistical noise of our simulations, the CHH strategy enables phase estimation approaching the QCRB within the full interval $\theta \in [0, \pi)$, as seen in the zoom in Figure 9 (b). For a more rigorous analysis of the convergence of the CHH strategy Appendix 8.4 discusses the proof of the asymptotic convergence of the CHH strategy to the QCRB over the full range $[0, \pi)$.

As a final step, we investigate the CHH measurement strategy under channel losses. Fig. 10 shows the normalized Holevo variance of the estimator obtained through the CHH estimation strategy with $m = 15$ adaptive steps each with $\nu = 247$ probe states with a squeezing strength $r = 1.01$. The loss is characterized by the channel transmission T for $T = 1$ in brown (lossless), $T = 0.99$ in light blue, and $T = 0.95$ in purple. The shaded regions represent one standard deviation. The dotted-dashed lines represent the minimum Cramér-Rao bound (CRB) for the homodyne measurement for different channel transmissions T, obtained as the inverse of the classical Fisher information in Eq. (25), and normalized to the QCRB. The dashed lines represent the QCRB for different channel transmissions T, which is obtained as the inverse of Eq. (24). We note that for a lossless channel $T = 1$, the CRB equals the QCRB due to the local optimality of homodyne measurements. We observe that the performance of the CHH strategy is close to the homodyne CRB (dotted-dashed) for the channel transmissions considered, and it is expected to approach this bound for all cases. Moreover, the performance of the CHH strategy is maintained for all the phases within the full range $[0, \pi)$ for squeezed vacuum.

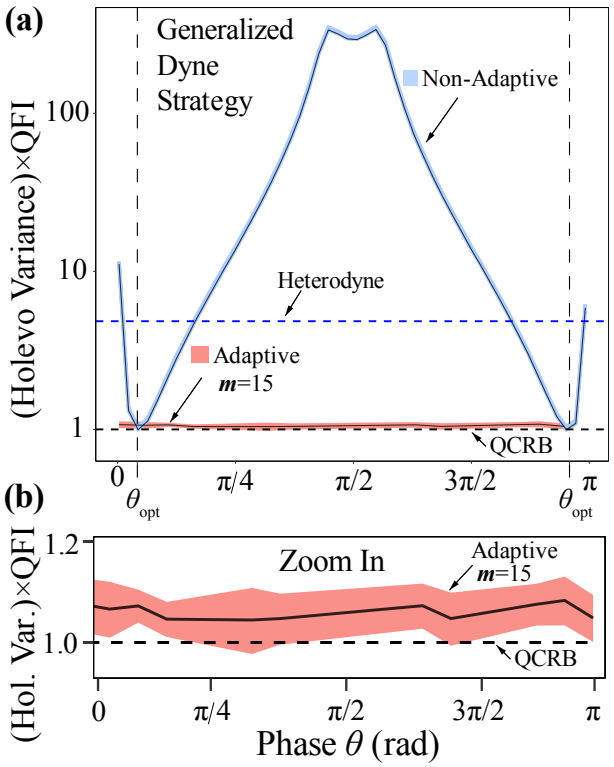

Figure 9: **(a)** Performance of the CHH phase estimation strategy with $m = 15$ adaptive steps (orange), using $N = 3705$ probes with $r = 1.01$. The performance of homodyne detection without feedback (blue) is shown for reference. In the CHH strategy, the initial adaptive step involves heterodyne sampling, while the subsequent adaptive steps utilize locally optimal homodyne POVMs in Eq. (16). Throughout the simulation, the sample size remains constant at $\nu = 247$ (number of probe states per adaptive step). The dashed blue line shows the heterodyne limit, while the dashed black line corresponds to the QCRB. The shaded regions indicate a one standard deviation. **(b)** Zoom in the region close to the QCRB.

7 Discussion & Conclusions

Our analysis and numerical simulations show that the proposed adaptive estimation strategy efficiently extracts the maximum attainable information about the unknown phase encoded in squeezed vacuum states in the asymptotic limit. However, we note that while the proposed strategy allows for phase estimation at the quantum limit for the full range of phases $[0, \pi)$ for squeezed vacuum states, this range is limited due to the π phase-shift symmetry inherent to these states. We also note that other quantum states used for phase estimation at the quantum limit such as NOON states face the same limitation due to their inherent phase-shift symmetries [12]. On the other hand, there may be other optical probes capable of solving the non-identifiability problem in the phase encoding due to state symmetries, albeit with lower QFI. Coherent states, for example, have a significantly lower QFI compared to squeezed vacuum states, but allow for unambiguously identifying the quadrants of the phase within $[0, 2\pi)$ [66–69].

As an alternative quantum probe for phase estimation, displaced squeezed states $D(\alpha)|0, r\rangle$ can offer the ability to unambiguously encode phases within $[0, 2\pi)$ with a higher QFI compared to coherent states. We note, however, that there will be a trade-off between the achievable QFI compared to that of squeezed vacuum states and the ability to identify the quadrants of the phase. Finding the best trade off requires op-

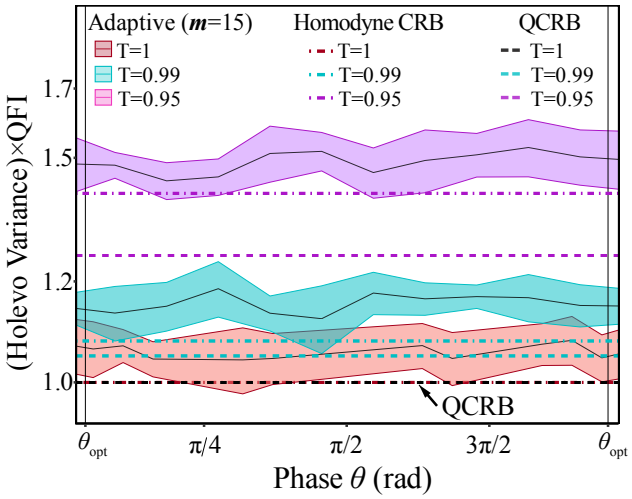

Figure 10: Performance of the CHH strategy under losses, with $m = 15$ adaptive steps and $N = 3705$ probes with $r = 1.01$. Losses are characterized by the channel transmission T for $T = 1$ in brown (lossless), $T = 0.99$ in light blue, and $T = 0.95$ in purple. The dotted-dashed lines represent the minimum CRB for the homodyne measurement normalized to the QCRB, i.e. $F_Q^{\text{Lossy}}/F_X^{\text{Lossy}}(\theta_{\text{opt}})$. The dashed lines represent the QCRB for different channel transmissions T. For $T = 1$, the homodyne CRB equals the QCRB due to the local optimality of the homodyne measurement.

timization of both the squeezing strength r and the displacement parameter α, given a fixed resource budget in terms of the number of photons. Moreover, this trade-off will critically depend on the available resources and experimental constraints. Further research will focus on exploring and identifying the optimal quantum probe states capable of overcoming the non-identifiability problem while maintaining a high QFI for phase estimation.

In summary, we propose a Gaussian estimation strategy for optical phase estimation with squeezed vacuum states that approaches the quantum limit in precision. This strategy leverages homodyne measurements and rotations to implement a complete set of locally optimal POVMs. This set of POVMs are used to construct an adaptive estimation method based on the Adaptive Quantum State Estimation (AQSE) formalism, which ensures consistency and efficiency of the estimator in the asymptotic limit, with variance equal to the inverse of the QFI for phases $\theta \in [0, \pi/2)$. To extend the parameter range for phase estimation to $[0, \pi)$, which is the maximum range of phases that can be encoded in squeezed vacuum states, we generalize the estimation strategy to incorporate a small number of heterodyne measurements. This heterodyne sampling allows for identifying the neighborhood of the phase within $[0, \pi)$, solving the non-identifiability problem in the likelihoods from homodyne measurements, while maintaining a quantum-optimal performance in the limit of many adaptive steps. This result represents a significant advancement in high-precision quantum metrology and optical phase estimation based on quantum correlated states.

8 Appendix

8.1 Efficiency and consistency of MLE in quantum systems

This appendix describes the conditions under which the MLE used in AQSE is consistent and efficient over the complete parameter space Θ. Let us consider the problem of estimating an unknown parameter $\theta \in \Theta$ associated with a set of quantum states $\{\rho(\theta) : \theta \in \Theta\}$ from measurements of the system. When independent measurements are performed over the system, a set of independent random variables $\vec{X}_N = X_1, \ldots, X_N \in \mathcal{X}^N$, $N \geq 1$ carry the information about θ. In this case, the total Fisher information about θ is the sum of the individual Fisher information values for each measurement. This property can be exploited to reach the QCRB in the asymptotic limit ($N \to \infty$). When the outcomes of a POVM M have a Fisher information that coincides with the QFI, and their probability distribution satisfies a set of mild regularity conditions described below, it can be shown that, in the asymptotic limit, the MLE applied to the outcomes of M can achieve the QCRB [27].

To saturate the QCRB, the MLE requires to be asymptotically consistent, which means that as the sample size increases, the MLE converges to the true value of the parameter θ in probability (weak sense) or almost surly (strong sense) [31]. For a MLE to be asymptotically consistent, the following conditions over the parametric set Θ and the set of density functions $\{f(X_i \mid \theta; M_i)\}_{\theta \in \Theta}$ for each POVM M_i must be satisfied [27, 31, 65]:

- **Compactness:** The parameter space Θ and the space of POVMs must be compact, which means that it is closed and bounded. This property ensures that the MLE exists for any sample size.
- **Identifiability:** The true value of the parameter must be uniquely determined by the probability distribution. In other words, different values of the parameter must produce different probability distributions.
- **Measurability:** The probability density function $f(X_i \mid \theta; M_i)$ must be measurable for all $X_i = x_i$ and for each POVM M_i. Thus the MLE is well-defined as a random variable.
- **Continuity:** The probability density function $f(X_i \mid \theta; M_i)$ must be continuous in the parameter space Θ for all $X_i = x_i$ and for each POVM M_i. This guarantees that small changes in the value of the parameter result in small changes in the probability.

- **Dominance:** The log likelihood $\log\left[f(X_i \mid \theta; M_i)\right]$ is uniformly Lipschitz in θ with respect to some dominating measure on $\mathcal{X}$. This provide the convergence of the MLE.

Under this set of regularity conditions, the MLE exhibits asymptotic consistency. As a result, assuming sufficiently smooth likelihoods, the distribution of the MLE in the limit $N \to \infty$ follows a normal distribution:

$$\widehat{\theta}(\vec{X}_N) \sim \mathcal{N}\left(\theta, \frac{1}{F_{\vec{X}_N}(\theta)}\right). \tag{28}$$

Here $\widehat{\theta}(\vec{X}_N)$ denotes the MLE based on the sample $\vec{X}_N$, and $F_{\vec{X}_N}(\theta)$ represents the Fisher information associated with the sample. Consequently, the variance of $\widehat{\theta}(\vec{X}_N)$ is given by $\frac{1}{F_{\vec{X}_N}(\theta)}$, and $\widehat{\theta}(\vec{X}_N)$ achieves the classical Cramér-Rao bound for all $\theta \in \Theta$. Notably, when the Fisher information of the random variables $\vec{X}_N$ equals the QFI, the MLE attains the QCRB, which corresponds to the ultimate limit in precision for parameter estimation. Based on this observation, the AQSE framework can be exploited to construct an asymptotically optimal strategy using homodyne detection. By satisfying the regularity conditions outlined above, the MLE is guaranteed to converge to the true value, and AQSE can be used to adapt the homodyne measurements to sample around the optimal point θ_{opt}, attaining the QCRB.

8.2 Proof of Convergence of the phase estimator variance to the QCRB

8.2.1 Asymptotic consistency of the MLE for the adaptive homodyne strategy

This appendix details the proof of the strong asymptotic consistency of the MLE obtained from the proposed adaptive homodyne strategy based on AQSE. As a first step, the adaptive strategy defines an initial estimate $\check{\theta}_1 \sim U\left(\tilde{\Theta}\right)$ for the parameter θ, where $\tilde{\Theta}$ is a compact subset of $(0, \pi/2)$. Then, the homodyne measurement with POVM $M_{\check{\theta}_1}$ in Eq. (17) yields a sample of measurement outcomes of size ν, $\vec{x}_\nu(\check{\theta}_1) = x_1(\check{\theta}_1), \ldots x_\nu(\check{\theta}_1)$. The MLE is then applied to this sample of measurement outcomes $\vec{x}_\nu(\check{\theta}_1)$ resulting in an updated estimate $\check{\theta}_1 := \widehat{\theta}_{\text{MLE}}\left(\vec{x}_\nu(\check{\theta}_1)\right)$. This new estimate serves as the subsequent guess of the parameter θ for the next adaptive step. Then, for a given subsequent adaptive step m, $m \geq 2$, the adaptive strategy performs the POVM $M_{\check{\theta}_m}$ yielding the sample of outcomes $\vec{x}_\nu(\check{\theta}_m) = x_1(\check{\theta}_m), \ldots x_\nu(\check{\theta}_m)$, from which the MLE produces an estimate $\widehat{\theta}_{\text{MLE}}\left(\vec{x}_\nu(\check{\theta}_1), \ldots, \vec{x}_\nu(\check{\theta}_m)\right) = \check{\theta}_{m+1}$. This procedure is repeated iteratively in subsequent adaptive measurements. By satisfying the regularity conditions described in Appendix: 8.1 for the statistical model for each homodyne measurement, we prove the *almost sure* convergence of the sequence of MLEs $\widehat{\theta}_{\text{MLE}}\left(\vec{X}_\nu(\check{\theta}_1), \ldots, \vec{X}_\nu(\check{\theta}_m)\right)$ to the true parameter θ as the number of adaptive steps $m \to \infty$.

First, we note that the set of homodyne measurements $\left\{M_{\check{\theta}}(dx)\right\}$ forms a set of locally optimal POVMs parameterized by $\tilde{\Theta}$. Without loss of generality, we assume that the true phase to be estimated is $\theta_0 \in \tilde{\Theta}$. For this proof, we assume that the regularity conditions described in Appendix 8.1 are satisfied. We first present a series of auxiliary **Lemmas 1 to 4**. Then we present the main result of this proof in **Theorem 5**, which shows the asymptotic consistency and convergence of the MLE. The method employed in this proof is analogous to the technique used to bound the probability of rejecting the null hypothesis in binary hypothesis testing based on the likelihood ratio test [31]. This technique has been applied to prove the asymptotic consistency to the MLE in the context of Optimal Design of Experiments [70] and in the context of quantum parameter estimation [27].

Let $\phi(\theta, \check{\theta}) = \theta + \theta_{\text{opt}} - \check{\theta}$ be the argument of the homodyne POVM in Eq. (17) for any θ, with $\check{\theta} \in \tilde{\Theta}$ and θ_{opt} defined in Eq. (15). For any $\epsilon > 0$, let the open neighborhood centered at θ and radius ϵ be:

$$N_\epsilon(\theta) = \{\theta' : |\theta' - \theta| < \epsilon\} = (\theta - \epsilon, \theta + \epsilon).$$

Let the log of the ratio of likelihoods be:

$$R(\theta, \theta_0, \check{\theta}) = \log\left(\frac{f(\vec{X}_\nu(\check{\theta}) \mid \phi(\theta, \check{\theta}))}{f(\vec{X}_\nu(\check{\theta}) \mid \phi(\theta_0, \check{\theta}))}\right),$$

and

$$R(\epsilon, \theta, \theta_0, \check{\theta}) = \sup_{\theta' \in N_\epsilon(\theta)} R(\theta', \theta_0, \check{\theta}),$$

where $f(x \mid \theta)$ is defined in Eq. (11) for any $\theta \in \tilde{\Theta}$.

Lemma 1. *For any $\theta, \theta_0 \in \tilde{\Theta}$ with $\theta \neq \theta_0$, it follows that:*

$$\left[\frac{2\sigma\left(\phi(\theta, \check{\theta})\right)\sigma\left(\phi(\theta_0, \check{\theta})\right)}{\sigma^2\left(\phi(\theta, \check{\theta})\right) + \sigma^2\left(\phi(\theta_0, \check{\theta})\right)}\right]^{1/2} < 1, \tag{29}$$

where $\sigma(\theta)$ is defined in Eq. (12) for the probability density function in Eq. (11) of the outcomes of homodyne measurements.

Proof.

$$\left[\frac{2\sigma\left(\phi(\theta,\check{\theta})\right)\sigma\left(\phi(\theta_0,\check{\theta})\right)}{\sigma^2\left(\phi(\theta,\check{\theta})\right)+\sigma^2\left(\phi(\theta_0,\check{\theta})\right)}\right]^{1/2} < 1$$
$$\iff 2\sigma\left(m(\theta,\check{\theta})\right)\sigma\left(m(\theta_0,\check{\theta})\right) < \sigma^2\left(m(\theta,\check{\theta})\right)+\sigma^2\left(m(\theta_0,\check{\theta})\right)$$
$$\iff \left(\sigma\left(\phi(\theta,\check{\theta})\right)-\sigma\left(\phi(\theta_0,\check{\theta})\right)\right)^2 > 0,$$

which holds from the identifiability condition. □

Lemma 2. *For any $\theta \in \tilde{\Theta}$ with $\theta \neq \theta_0$, it follows that:*

$$g(\theta) = \sup_{\check{\theta}\in\tilde{\Theta}} \mathrm{E}_{\theta_0}\left[e^{\left(R(\theta,\theta_0,\check{\theta})\right)^{1/2}}\right] < 1. \tag{30}$$

Proof.

$$\begin{aligned} g(\theta) &= \sup_{\check{\theta}\in\tilde{\Theta}} \int_{\mathbb{R}^\nu} \sqrt{f\left(\vec{x}_\nu(\check{\theta}) \mid \phi(\theta,\check{\theta})\right) f\left(\vec{x}_\nu(\check{\theta}) \mid \phi(\theta_0,\check{\theta})\right)}\, d\vec{x}_\nu(\check{\theta}) \\ &= \sup_{\check{\theta}\in\tilde{\Theta}} \int_{\mathbb{R}^\nu} \frac{e^{-\sum_{j=1}^{\nu}\frac{x_j^2}{4}\frac{\sigma^2(\phi(\theta,\check{\theta}))+\sigma^2(\phi(\theta_0,\check{\theta}))}{\sigma^2(\phi(\theta,\check{\theta}))\sigma^2(\phi(\theta_0,\check{\theta}))}}}{\left[2\pi\sigma\left(\phi(\theta,\check{\theta})\right)\sigma\left(\phi(\theta_0,\check{\theta})\right)\right]^{\nu/2}} d\vec{x}_\nu(\check{\theta}) \\ &= \sup_{\check{\theta}\in\tilde{\Theta}} \left[\frac{2\sigma\left(\phi(\theta_0,\check{\theta})\right)\sigma\left(\phi(\theta,\check{\theta})\right)}{\sigma^2\left(\phi(\theta,\check{\theta})\right)+\sigma^2\left(\phi(\theta_0,\check{\theta})\right)}\right]^{\nu/2}. \end{aligned}$$

Since $\tilde{\Theta}$ is compact, the set $\tilde{\Theta}$ contains its supremum. Then there exits a point $\check{\theta}_{\sup} \in \tilde{\Theta}$ such that

$$\sup_{\check{\theta}\in\tilde{\Theta}} \left[\frac{2\sigma\left(\phi(\theta,\check{\theta})\right)\sigma\left(\phi(\theta_0,\check{\theta})\right)}{\sigma^2\left(\phi(\theta,\check{\theta})\right)+\sigma^2\left(\phi(\theta_0,\check{\theta})\right)}\right]^{\nu/2} = \left[\frac{2\sigma\left(\phi(\theta,\check{\theta}_{\sup})\right)\sigma\left(\phi(\theta_0,\check{\theta}_{\sup})\right)}{\sigma^2\left(\phi(\theta,\check{\theta}_{\sup})\right)+\sigma^2\left(\phi(\theta_0,\check{\theta}_{\sup})\right)}\right]^{\nu/2},$$

with $\tilde{\theta}^{\sup} = \theta+\theta_{\mathrm{opt}}-\check{\theta}_{\sup}$ and $\tilde{\theta}_0^{\sup} = \theta_0+\theta_{\mathrm{opt}}-\check{\theta}_{\sup}$. Therefore the proof of Eq. (30) follows from Eq. (29) in **Lemma 1**. □

Lemma 3. *Let $\bar{S}^\epsilon(\check{\theta}) = \mathrm{E}_{\theta_0}\left[e^{R(\epsilon,\theta,\theta_0,\check{\theta})^{1/2}}\right]$ and $\bar{S}(\check{\theta}) = \mathrm{E}_{\theta_0}\left[e^{R(\theta,\theta_0,\check{\theta})^{1/2}}\right]$ for any $\theta \in \tilde{\Theta}$ with $\theta \neq \theta_0$. Then $\lim_{\epsilon\downarrow 0}\bar{S}^\epsilon(\check{\theta}) = \bar{S}(\check{\theta})$, and the following inequality holds:*

$$\limsup_{\epsilon\downarrow 0}\sup_{\check{\theta}\in\tilde{\Theta}} \bar{S}^\epsilon(\check{\theta}) < 1. \tag{31}$$

Proof. Given that

$$\bar{S}^\epsilon(\check{\theta}) = \int_{\mathbb{R}^\nu} \sup_{\theta'\in N_\epsilon(\theta)} \sqrt{f\left(\vec{x}_\nu(\check{\theta}) \mid \phi(\theta',\check{\theta})\right) f\left(\vec{x}_\nu(\check{\theta}) \mid \phi(\theta_0,\check{\theta})\right)}\, d\vec{x}_\nu(\check{\theta}),$$

by the continuity of the density function, it follows that $\lim_{\epsilon\downarrow 0}\bar{S}^\epsilon(\check{\theta}) = \bar{S}(\check{\theta})$ for any $\theta \in \tilde{\Theta}$. Moreover, the closure of $N_\epsilon(\theta)$, $\overline{N_\epsilon(\theta)} \subset \tilde{\Theta}$ is compact, because $\tilde{\Theta}$ itself is a compact set. Consequently,

$$\bar{S}^\epsilon(\check{\theta}) = \int_{\mathbb{R}^\nu} \max_{\theta'\in\overline{N_\epsilon(\theta)}} \sqrt{f\left(\vec{x}_\nu(\check{\theta}) \mid \phi(\theta',\check{\theta})\right) f\left(\vec{x}_\nu(\check{\theta}) \mid \phi(\theta_0,\check{\theta})\right)}\, d\vec{x}_\nu(\check{\theta}).$$

We note that the function

$$\sqrt{f\left(\vec{x}_\nu(\check{\theta}) \mid \phi(\theta',\check{\theta})\right) f\left(\vec{x}_\nu(\check{\theta}) \mid \phi(\theta_0,\check{\theta})\right)}$$

is continuous over the Cartesian product of the compact sets $\overline{N_\epsilon(\theta)} \times \tilde{\Theta}$, which is also compact. Then the integrand in $\bar{S}^\epsilon(\check{\theta})$ is a continuous function at $\check{\theta}$ [27, 71]. Therefore, the sequence of functions $\left(\bar{S}^\epsilon(\check{\theta})\right)_{\epsilon\downarrow 0}$ forms a monotonically decreasing sequence of continuous functions defined on the compact set $\tilde{\Theta}$.

By Dini's theorem [71], the convergence from $\bar{S}^{\epsilon}(\check{\theta}) \to \bar{S}(\check{\theta})$ as $\epsilon \downarrow 0$ is uniform in θ. As a consequence,

$$\lim_{\epsilon \downarrow 0} \sup_{\theta \in \tilde{\Theta}} \bar{S}^{\epsilon}(\check{\theta}) = \sup_{\theta \in \tilde{\Theta}} \lim_{\epsilon \downarrow 0} \bar{S}^{\epsilon}(\check{\theta}) = \sup_{\theta \in \tilde{\Theta}} \bar{S}(\check{\theta}) = g(\theta),$$

which, according to Eq. (30) in **Lemma 2**, is less than 1. □

Lemma 4. *For any $\theta \in \tilde{\Theta}$ with $\theta \neq \theta_0$, there exist $\epsilon > 0$ and $b > 0$ such that for any $m \in \mathbb{N}$, and any set of homodyne measurements parameterized by $\left\{\check{\theta}_i\right\}_{1 \leq i \leq m} \subset \tilde{\Theta}$, the following inequality holds*

$$P_{\theta_0}\left(\sum_{i=1}^{m} R(\epsilon, \theta, \theta_0, \check{\theta}_i) > 0\right) \leq e^{-bm},\ m \geq 1. \quad (32)$$

Proof. We start by observing that

$$\begin{aligned} P_{\theta_0}\left[\sum_{i=1}^{m} R(\epsilon, \theta, \theta_0, \check{\theta}_i) > 0\right] &= P_{\theta_0}\left[e^{\sum_{i=1}^{m} R(\epsilon,\theta,\theta_0,\check{\theta}_i)} > 1\right] \\ &= P_{\theta_0}\left[e^{\frac{1}{2}\sum_{i=1}^{m} R(\epsilon,\theta,\theta_0,\check{\theta}_i)} > 1\right] \\ &= P_{\theta_0}\left[\prod_{i=1}^{m} e^{R(\epsilon,\theta,\theta_0,\check{\theta}_i)/2} > 1\right]. \end{aligned}$$

Applying the Markov's inequality, we obtain

$$P_{\theta_0}\left[\prod_{i=1}^{m} e^{R(\epsilon,\theta,\theta_0,\check{\theta}_i)/2} > 1\right] \leq \mathrm{E}_{\theta_0}\left[\prod_{i=1}^{m} e^{R(\epsilon,\theta,\theta_0,\check{\theta}_i)/2}\right]. \quad (33)$$

We note that Eq. (31) implies that there exist sufficiently small $\epsilon > 0$ and $b > 0$ such that

$$\sup_{\check{\theta} \in \tilde{\Theta}} \bar{S}^{\epsilon}(\check{\theta}) = e^{-b} < 1. \quad (34)$$

Let $Z_i = e^{R(\epsilon,\theta,\theta_0,\check{\theta}_i)/2}$ for $1 \leq i \leq m$, and $Z_0 = 1$. We can define a stochastic process

$$Y_m = \prod_{i=0}^{m} Z_m,\ m \geq 0.$$

This sequence of independent and non-negative random variables $\{Y_m\}_{m \geq 0}$ forms an adapted stochastic process relative to the filtered space $(\Omega, \mathcal{F}, \{\mathcal{F}_m\}, P)$, where $\{\mathcal{F}_m; m \geq 0\}$ is the natural filtration, $\mathcal{F}_0 := (\emptyset, \Omega)$, and $\mathcal{F}_m := \sigma\left(\vec{X}_\nu(\check{\theta}_1), \vec{X}_\nu(\check{\theta}_2), \ldots, \vec{X}_\nu(\check{\theta}_m)\right)$ [72]. Furthermore, according to Eq. (29), this stochastic process decreases on average, almost surely (a.s.), as indicated by

$$\mathrm{E}_{\theta_0}\left[Z_m \mid \mathcal{F}_{m-1}\right] \leq Z_{m-1},\ m \geq 1,$$

where the conditional expectation is well defined, since Y_m is a $\mathcal{F}_m$-measurable function. Consequently, the sequence $\{Y_m\}_{m \geq 0}$ consists of non-negative independent random variables that satisfies the supermartingale condition [72]. Hence by the tower property of supermartingales, together with Eq. (34), for $m \geq 1$ and for a sufficiently small $\epsilon > 0$, we have

$$\begin{aligned} \mathrm{E}_{\theta_0}\left[Y_m \mid \mathcal{F}_{m-1}\right] &= \mathrm{E}_{\theta_0}\left[Y_{m-1} Z_m \mid \mathcal{F}_{m-1}\right] \\ &= Y_{m-1} \mathrm{E}_{\theta_0}\left[Z_m \mid \mathcal{F}_{m-1}\right] \\ &\leq Y_{m-1} e^{-b}. \end{aligned}$$

The iteration of this expectation through the filtration levels yields:

$$\mathrm{E}_{\theta_0}\left[Y_m\right] = \mathrm{E}_{\theta_0}\left[Y_m \mid \mathcal{F}_{m-1} \mid \mathcal{F}_{m-2} \mid \cdots \mid \mathcal{F}_0\right] \leq e^{-bm}.$$

Finally, incorporating this inequality into Eq. (33), we conclude the proof. □

Theorem 5 (Asymptotic strong consistency)**.** *Let $\theta_0 \in \tilde{\Theta}$ be the true value of the phase, and be an interior point of $\tilde{\Theta}$. Consider $\left\{\widehat{\theta}(\vec{X}_\nu\left(\check{\theta}_1), \ldots, \vec{X}_\nu(\check{\theta}_m)\right)\right\}_{1 \leq i \leq m}$ a sequence of MLEs over m adaptive steps, defined by AQSE over the set of homodyne measurements $\left\{M_{\check{\theta}_i}(dx)\right\}_{1 \leq 1 \leq m}$. Then,*

$$\widehat{\theta}\left(\vec{X}_\nu(\check{\theta}_1), \ldots, \vec{X}_\nu(\check{\theta}_m)\right) \xrightarrow{a.s.} \theta_0 \text{ as } m \to \infty. \quad (35)$$

Proof. Let

$$S_m(\theta_0, \theta) = \sum_{i=1}^{m} R(\theta, \theta_0, \check{\theta}_i)$$

and

$$S_m^{\epsilon}(\theta_0, \theta) = \sum_{i=1}^{m} R(\epsilon, \theta, \theta_0, \check{\theta}_i).$$

For any $a \geq 0$, let

$$N_a(\theta_0)^c = \left\{\theta \in \tilde{\Theta} : |\theta - \theta_0| \geq a\right\}.$$

Given that $\tilde{\Theta}$ is compact, then $N_a(\theta_0)^c$ is also compact. Then, for every arbitrary collection $\mathcal{K}$ of open intervals of $\tilde{\Theta}$, such that

$$N_a(\theta_0)^c \subseteq \cup_{K \in \mathcal{K}} K,$$

there exits a finite subcollection $\mathcal{J} \subseteq \mathcal{K}$ such that

$$N_a(\theta_0)^c \subseteq \cup_{J \in \mathcal{J}} J.$$

Each $J \in \mathcal{J}$ can be represented as a neighborhood $N_{\epsilon_i}(\theta_i)$ for some $\theta_i \in \tilde{\Theta}$ and $\epsilon_i > 0$. Therefore, for some finite set $\{\theta_1, \ldots, \theta_j\}$,

$$N_a(\theta_0)^c \subseteq \cup_{\theta \in \{\theta_1, \ldots, \theta_j\}} N_{\epsilon_i}(\theta_i),$$

where the ϵ_i's are chosen such that Eq. (32) in **Lemma 4** holds for every θ_i and its corresponding b_i, with $i = 1, \ldots, j$.

The next step in this proof consists of bounding the probability that the estimator $\widehat{\theta}$ after m adaptive measurements is at a distance larger than or equal to a from the true value θ_0, i.e.,

$$\left|\widehat{\theta}\left(\vec{X}_\nu(\check{\theta}_1),\ldots,\vec{X}_\nu(\check{\theta}_m)\right)-\theta_0\right|\geq a.$$

This occurs when the maximum of the likelihood function $L_m(\theta)=\prod_{i=1}^m f(\vec{X}_\nu(\check{\theta}_i)\mid\phi(\theta,\check{\theta}_i))$ belongs to $N_a(\theta_0)^c$. This would imply that $L_m(\widehat{\theta})>L(\theta_0)$ and hence

$$\sup_{\theta\in N_a(\theta_0)^c}\prod_{i=1}^m\frac{f\left(\vec{X}_\nu(\check{\theta}_i)\mid\phi(\theta,\check{\theta}_i)\right)}{f\left(\vec{X}_\nu(\check{\theta}_i)\mid\phi(\theta_0,\check{\theta}_i)\right)}>1.$$

Thus

$$\begin{aligned}
P_{\theta_0}\left(\left|\widehat{\theta}\left(\vec{X}_\nu(\check{\theta}_1),\ldots,\vec{X}_\nu(\check{\theta}_m)\right)-\theta_0\right|\geq a\right)&=P_{\theta_0}\left(\sup_{\theta\in N_a(\theta_0)^c}\prod_{i=1}^m\left[\frac{f\left(\vec{X}_\nu(\check{\theta}_i)\mid\phi(\theta,\check{\theta}_i)\right)}{f\left(\vec{X}_\nu(\check{\theta}_i)\mid\phi(\theta_0,\check{\theta}_i)\right)}\right]>1\right)\\
&=P_{\theta_0}\left(\sup_{\theta\in N_a(\theta_0)^c}\sum_{i=1}^m\log\left[\frac{f\left(\vec{X}_\nu(\check{\theta}_i)\mid\phi(\theta,\check{\theta}_i)\right)}{f\left(\vec{X}_\nu(\check{\theta}_i)\mid\phi(\theta_0,\check{\theta}_i)\right)}\right]>0\right)\\
&=P_{\theta_0}\left(\sup_{\theta\in N_a(\theta_0)^c}S_m(\theta_0,\theta)>0\right)\\
&\leq P_{\theta_0}\left(\max_{1\leq i\leq j}S_m^{\epsilon_i}(\theta_0,\theta_i)>0\right)\\
&\leq j\exp\left[-\min_{1\leq i\leq j}[b_i]\,m\right],\ m\geq 1.
\end{aligned}$$

In the third step of the previous sequence of equations, we have used the fact that the logarithm is a strictly increasing function, and that $\tilde{\Theta}$ is compact, to commute the supremum with the logarithm. To bound the probability P_{θ_0} in the last step of the sequence of equations, we have used Eq. (32) in **Lemma 4**.

Finally, by the Borell Cantelli lemma [73], we conclude that

$$P_{\theta_0}\left(\left|\widehat{\theta}\left(\vec{X}_\nu(\check{\theta}_1),\ldots,\vec{X}_\nu(\check{\theta}_m)\right)-\theta_0\right|\geq a\quad\text{i.o.}\right)=0,$$

were i.o. stands for *infinitely often*. Therefore, $\widehat{\theta}\left(\vec{X}_\nu(\check{\theta}_1),\ldots,\vec{X}_\nu(\check{\theta}_m)\right)\xrightarrow{a.s.}\theta_0$ as $m\to\infty$. □

Corollary 5.1. $\widehat{\theta}\left(\vec{X}_\nu(\check{\theta}_1),\ldots,\vec{X}_\nu(\check{\theta}_m)\right)=\theta_0+o_P(1)$.

Proof. Let $(W_m)_{m\geq 1}$ be a sequence of random variables. If $W_m=o_p(1)$, then the stochastic sequence $(W_m)_{m\geq 1}$ converges in probability to 0 [74]. It implies that with arbitrary high probability, $|W_m|=o(1)$. Specifically, for any $\epsilon,\delta>0$, there exists $N_0(\epsilon,\delta)$, such that for any $m>N_0(\epsilon,\delta)$,

$$P\left(|W_m|<\epsilon\right)\geq 1-\delta. \tag{36}$$

On the other hand, Eq. (35) in **Theorem 5** guarantees the almost sure convergence for the sequence of MLEs $\left(\widehat{\theta}\left(\vec{X}_\nu(\check{\theta}_1),\ldots,\vec{X}_\nu(\check{\theta}_m)\right)\right)_{m\geq 1}$ to θ_0. Almost sure convergence implies convergence in probability [31]. Therefore, we can conclude that $\widehat{\theta}\left(\vec{X}_\nu(\check{\theta}_1),\ldots,\vec{X}_\nu(\check{\theta}_m)\right)-\theta_0=o_P(1)$ as the number of adaptive steps m increases. □

This means that the sequence of MLEs $\left(\widehat{\theta}(\vec{X}_\nu(\check{\theta}_1),\ldots,\vec{X}_\nu(\check{\theta}_m))\right)_{m\geq 1}$ gets arbitrarily close to θ_0 with increasing probability as m becomes very large [74].

8.2.2 Saturation of the QCRB

A consequence of the *almost sure convergence* of the MLE described in Appendix 8.2.1 is that the distribution of the sequence of MLEs converges to a normal distribution (asymptotic normality) with variance equal to the inverse of the QFI as the number of adaptive steps tends to infinity. To prove this statement we follow a similar methodology as in the case of i.i.d. random variables [31]. However, in our case, the measurement samples $\vec{X}_\nu(\check{\theta}_1),\ldots,\vec{X}_\nu(\check{\theta}_m)$ are not identically distributed. Moreover, this proof requires the additional assumption that the likelihood functions $f(\vec{X}_\nu(\check{\theta})\mid\phi(\theta,\check{\theta}))$ are sufficiently smooth and continuous on $\mathbb{R}^\nu\times\tilde{\Theta}\times\tilde{\Theta}$. This assumption ensures that the existence of the Fisher information at every point in $\mathbb{R}^\nu\times\tilde{\Theta}\times\tilde{\Theta}$.

Under the regularity conditions described in Appendix 8.1 and with the additional assumption of sufficient smoothness of the likelihood functions, we expand the derivative of the logarithm of the likelihood $l_m(\theta) = \sum_{i=1}^{m} \log\left[f(\vec{X}_\nu(\check{\theta}_i) \mid \phi(\theta, \check{\theta}_i))\right]$ about θ_0 up to second order, yielding

$$l'_m(\theta) = l'_m(\theta_0) + l''_m(\theta_0)(\theta - \theta_0) + \frac{1}{2} l'''_m(\theta^*)(\theta - \theta_0)^2, \tag{37}$$

where $\theta^* \in \tilde{\Theta}$ such that $|\theta^* - \theta_0| < |\theta - \theta_0|$. Here, the regularity conditions in Appendix: 8.1 ensure that the estimates from $\widehat{\theta}(\vec{X}_\nu(\check{\theta}_1), \ldots, \vec{X}_\nu(\check{\theta}_m))$ are stationary points of the likelihood function. Then, when evaluating Eq. (37) at $\theta = \widehat{\theta}(\vec{X}_\nu(\check{\theta}_1), \ldots, \vec{X}_\nu(\check{\theta}_m))$, the left-hand side of this equation vanishes, yielding

$$\sqrt{m}\left(\widehat{\theta}(\vec{X}_\nu(\check{\theta}_1), \ldots, \vec{X}_\nu(\check{\theta}_m)) - \theta_0\right) = \frac{\frac{l'_m(\theta_0)}{\sqrt{m}}}{-\frac{l''_m(\theta_0)}{m} - \frac{l'''_m(\theta^*)}{2m}\left(\widehat{\theta}(\vec{X}_\nu(\check{\theta}_1), \ldots, \vec{X}_\nu(\check{\theta}_m)) - \theta_0\right)}. \tag{38}$$

Moreover, given that the MLE is asymptotically consistent, i.e., $\widehat{\theta}\left(\vec{X}_\nu(\check{\theta}_1), \ldots, \vec{X}_\nu(\check{\theta}_m)\right) \xrightarrow{\text{a.s.}} \theta_0$, and the smoothness of the likelihood, it can be shown that [27]:

(a) $l'_m(\theta_0)/\sqrt{m} \to \mathcal{N}(0, 1/\nu F_X(\theta_{\text{opt}}))$ in distribution,

(b) (b) $l''_m(\theta_0)/m \to -\nu F_X(\theta_{\text{opt}})$ in probability, and

(c) $l'''_m(\theta^*)/m$ is bounded in probability.

This results in the asymptotic normality of the estimator:

$$\sqrt{m}\left(\widehat{\theta}\left(\vec{X}_\nu(\check{\theta}_1), \ldots, \vec{X}_\nu(\check{\theta}_m)\right)\right) \xrightarrow{\text{d}} \mathcal{N}\left(\theta_0, \frac{1}{\nu F_Q}\right), \tag{39}$$

where the d above the arrow denotes convergence in distribution. Therefore, the distribution of the estimator follows a normal distribution with mean equal to θ_0 and a variance equal to the inverse of the QFI, and therefore saturates the QCRB $[NF_X(\theta_{\text{opt}})]^{-1}$ in the asymptotic limit of $m \to \infty$, with $N = \nu \times m$.

We can give the bound for the rate of convergence using asymptotic normality. Similar to how the definition of o_p states the convergence in probability, if a sequence of random variables $W_m = O_p(a_m)$, then with high probability, $|W_m| = O(a_m)$ (i.e. for sufficiently large m, the sequence W_m is bounded above by a constant multiple of the sequence a_m in probability) [74]. Specifically, for every $\epsilon > 0$ there exists a constant $K(\epsilon)$ and an integer $N_0(\epsilon)$ such that if $m > N_0(\epsilon)$, then

$$P\left(\left|\frac{W_m}{a_m}\right| \leq K(\epsilon)\right) \geq 1 - \epsilon. \tag{40}$$

Since Eq. (39) holds for $W_m = \widehat{\theta} - \theta_0$, we can apply the Chebyshev inequality [31]. This inequality states that for any $\epsilon > 0$, we can choose a constant $K(\epsilon) = 1/\sqrt{\epsilon} > 0$ such that for a sufficiently large m,

$$P_\theta\left(\left|\sqrt{m}\left(\widehat{\theta}\left(\vec{X}_\nu(\check{\theta}_1), \ldots, \vec{X}_\nu(\check{\theta}_m)\right) - \theta_0\right)\right| < K(\epsilon)\right) \geq 1 - \epsilon. \tag{41}$$

Therefore, we find that $\widehat{\theta}\left(\vec{X}_\nu(\check{\theta}_1), \ldots, \vec{X}_\nu(\check{\theta}_m)\right) - \theta_0 = O_p(1/\sqrt{m})$.

8.3 Phase estimation around θ_{opt}

The estimator in Eq. (21) of the proposed adaptive homodyne strategy minimizes the variance over all the phases within the parametric space from $[0, \pi/2)$. This estimator yields a variance above the QCRB for phases close to θ_{opt} for a small number of adaptive steps m. On the other hand, we note that the two-step protocol from Ref. [22] is closer to the QCRB for $\theta \approx \theta_{opt}$ than our strategy for small $m = 3, 5$. However, our proposed strategy is more general, and encompasses the one from Ref. [22]. By taking an uneven splitting ratio between the first and second step and $\check{\theta}_1 = \theta_{opt}$, our strategy with $m = 2$ reduces to the strategy from Ref. [22]. Nevertheless, by construction our strategy is guaranteed to achieve the QCRB for any phase in the asymptotic limit.

8.4 Convergence of the CHH strategy over the full range $[0, \pi)$

The asymptotic consistency of $\widehat{\theta}\left(\vec{X}_\nu(\check{\theta}_1), \ldots, \vec{X}_\nu(\check{\theta}_m)\right)$ can be extended to a compact parameter space $\tilde{\Theta} \subset [0, \pi)$ by replacing the initial step of sampling $\vec{X}_\nu(\check{\theta}_1)$ with a sample $\vec{X}_\nu^{(1)} \in \mathbb{C}^\nu$ of size ν obtained from a series of heterodyne measurements. This preliminary heterodyne sampling provides sufficient information about θ_0 to overcome the non-identifiability problem inherent to homodyne measurements, thereby allowing for extending the parameter space.

The proof of asymptotic consistency of the MLE and convergence of the estimator variance to the QCRB in Appendix 8.2 remains valid for the full range $[0, \pi)$ if we can show a new version of **Lemma 2**. This new **Lemma** incorporates the likelihood function from

the heterodyne measurement as a multiplicative factor in the likelihood function for the subsequent homodyne measurements. From this result, the remaining **Lemmas** 3, 4 and **Theorem** 5 in Appendix 8.2 for proving almost sure convergence of the MLE follow analogously.

Lemma 6. *For any $\theta \in \tilde{\Theta}$ with $\theta \neq \theta_0$, it follows that:*

$$g_{\mathrm{CHH}}(\theta) = \sup_{\check{\theta}\in\tilde{\Theta}} \mathrm{E}_{\theta_0}\left[e^{\left(R_{\mathrm{CHH}}(\theta,\theta_0,\check{\theta})\right)^{1/2}}\right] < 1, \tag{42}$$

where

$$R_{\mathrm{CHH}}(\theta,\theta_0,\check{\theta}) = \log\left(\frac{f\left(\vec{X}_\nu^{Het} \mid \theta\right) f(\vec{X}_\nu(\check{\theta}) \mid \phi(\theta,\check{\theta}))}{f\left(\vec{X}_\nu^{Het} \mid \theta\right) f(\vec{X}_\nu(\check{\theta}) \mid \phi(\theta_0,\check{\theta}))}\right),$$

Proof. Let $\vec{x}_\nu^{\mathrm{Het}} = \alpha_1,\ldots,\alpha_\nu$ be an observed sample from $\vec{X}_\nu^{\mathrm{Het}} \in \mathbb{C}^\nu$ and assume $\theta \neq \theta_0$ for $\theta,\theta_0 \in \tilde{\Theta}$. In this case,

$$\begin{aligned} g_{\mathrm{CHH}}(\theta) &= \sup_{\check{\theta}\in\tilde{\Theta}} \int_{\mathbb{C}^\nu} \sqrt{f\left(\vec{x}_\nu^{\mathrm{Het}} \mid \theta\right) f\left(\vec{x}_\nu^{\mathrm{Het}} \mid \theta_0\right)} d\vec{x}_\nu^{\mathrm{Het}} \int_{\mathbb{R}^\nu} \sqrt{f\left(\vec{x}_\nu(\check{\theta}) \mid \phi(\theta,\check{\theta})\right) f\left(\vec{x}_\nu(\check{\theta}) \mid \phi(\theta_0,\check{\theta})\right)}\, d\vec{x}_\nu(\check{\theta}) \\ &= \int_{\mathbb{C}^\nu} \sqrt{f\left(\vec{x}_\nu^{\mathrm{Het}} \mid \theta\right) f\left(\vec{x}_\nu^{\mathrm{Het}} \mid \theta_0\right)} d\vec{x}_\nu^{\mathrm{Het}} \times g(\theta), \end{aligned} \tag{43}$$

where $g(\theta)$ is defined in Eq. (30).

Since $g(\theta) < 1$ according to Lemma 2 in Appendix 8.2, then it suffices to show that:

$$\int_{\mathbb{C}^\nu} \sqrt{f\left(\vec{x}_\nu^{\mathrm{Het}} \mid \theta\right) f\left(\vec{x}_\nu^{\mathrm{Het}} \mid \theta_0\right)} d\vec{x}_\nu^{\mathrm{Het}} < 1, \tag{44}$$

For a heterodyne measurement outcomes $\vec{x}_\nu^{\mathrm{Het}}$, the likelihood function is expressed as

$$f(\vec{x}_\nu^{\mathrm{Het}} \mid \theta) = [\pi\cosh(r)]^{-\nu} \prod_{j=1}^{\nu} e^{-|\alpha_j|^2 - \tanh(r)\mathrm{Re}\left[\alpha_j^2 e^{i2\theta}\right]}. \tag{45}$$

Then, the integral of the square root of the product of the likelihoods for θ and θ_0 becomes

$$\begin{aligned} &\int_{\mathbb{C}^\nu} \sqrt{f\left(\vec{x}_\nu^{\mathrm{Het}} \mid \theta\right) f\left(\vec{x}_\nu^{\mathrm{Het}} \mid \theta_0\right)} d\vec{x}_\nu^{\mathrm{Het}} = [\pi\cosh(r)]^{-\nu} \prod_{j=1}^{\nu} \int_{\mathbb{C}} e^{-|\alpha_j|^2 - \frac{\tanh(r)}{2}\left(\mathrm{Re}\left[\alpha_j^2 e^{i2\theta}\right] - \mathrm{Re}\left[\alpha_j^2 e^{i2\theta_0}\right]\right)} d\alpha_j \\ &= [\pi\cosh(r)]^{-\nu} \prod_{j=1}^{\nu} \int_{\mathbb{R}^2} e^{-\left(a_j^2+b_j^2\right) - \tanh(r)\cos(\theta-\theta_0)\left[\cos(\theta+\theta_0)(a_j^2-b_j^2) - 2ab(\sin(2\theta)+\sin(2\theta_0))\right]} da_j db_j \\ &= \left[\cosh(r)\sqrt{1-\cos^2(\theta-\theta_0)\tanh^2(r)}\right]^{-\nu}. \end{aligned} \tag{46}$$

Since the term $\left[\cosh(r)\sqrt{1-\cos^2(\theta-\theta_0)\tanh^2(r)}\right]^{-1}$ <1 for $r>0$, the assertion follows. □

Since **Lemma 6** holds, the proof of the asymptotic consistency of the MLE and convergence to the QCRB proceeds analogously to the proof in Appendix 8.2.

8.4.1 Numerical tests of estimator normality for the CHH strategy over $[0,\pi)$.

Analogous to the case of adaptive homodyne in Section 3, the MLE from the CHH strategy is expected to show asymptotic normality, defined in Eq. (39). We tested the normality of the MLE over $[0,\pi)$. To this end, we conducted five independent Anderson–Darling goodness-of-fit tests on $N = 1000$ samples of $\sqrt{m}\left(\widehat{\theta}\left(\vec{X}_\nu^{\mathrm{Het}}, \vec{X}_\nu(\check{\theta}_2),\ldots,\vec{X}_\nu(\check{\theta}_m)\right) - \theta_0\right)$, with $m = 20$, and $\nu = 50$ for 5 randomly selected values of θ_0 within $[0,\pi)$. The null hypothesis for each test posited that the samples from the MLE follow a normal distribution $\mathcal{N}\left(\theta_0, \frac{1}{1000F_X(\theta_{\mathrm{opt}})}\right)$ with $r = 1$. Using the `DescTools` package in **R**, these tests produced a set of five p-values. Subsequently, the Fisher method, implemented in the package of R `poolr`, calculated a combined p-value of 0.9150486. Given this very high combined p-value, we fail to reject the null hypothesis that the samples follow the specified normal distribution. This study provides statistical evidence that the MLE reaches the asymptotic normality with a moderate number of adaptive steps, in this test $m = 20$ steps.

8.4.2 Degree of non-Gaussianity of the MLE for small m.

In general, the distribution of MLEs obtained from the CHH strategy is a non-Gaussian distribution for

small m, and is expected to approach a normal distribution as m increases. We investigate the degree of non-Gaussianity of the MLE for small m by studying the first four central moments of the estimator distribution from the CHH strategy as a function of m. Figure 11 shows (a) the first moment (bias), (b) the second moment (normalized Holevo variance), the third moment (skewness), and the fourth moment (excess of kurtosis), for the CHH strategy with $N = 3000$ and r. We observe that the bias quickly converges to zero, the variance approaches the QCRB, and both the skewness and excess kurtosis tend to zero as m increases. These results show that while for a small m the MLE shows non-Gaussian characteristics, such as a small asymmetry (skewness) and the presence of outliers (excess of kurtosis), the MLE tends to a normal distribution as m increases. These results highlight the importance of having a sufficiently large number of probe states N, and enough m, to ensure the convergence to the QCRB for any $\theta \in [0, \pi)$.

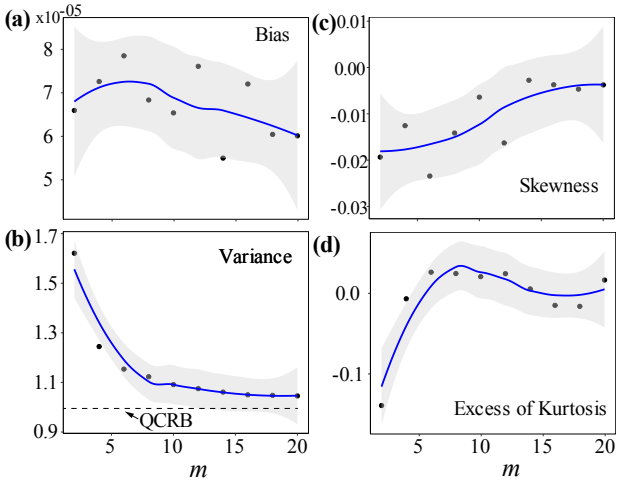

Figure 11: Degree of non-Gaussianity of the MLE for the CHH strategy with $N = 3000$ and $r = 1$. Each panel represents the evolution of one of the central moments of the estimator distribution as a function of the number of adaptive steps m. **(a)** First moment (Bias), **(b)** Second moment (normalized Holevo variance), **(c)** Third moment (Skewness), and **(d)** Fourth moment (excess of kurtosis). Black dots represent the average of 5 Monte Carlo simulations, each with 1×10^4 samples. The blue lines represent the tendencies provided by the localized regression method with span of 0.9, and the light-gray shadows represent the 95 percent confidence interval. Note that the bias rapidly converges to zero and the variance approaches the QCRB. The skewness and excess of kurtosis tend to zero as m increases.

Funding

This work was funded by the National Science Foundation (NSF) Grants # PHY-2210447, FRHTP # PHY-2116246, and the Q-SEnSE QLCI # 2016244.

Acknowledgments

We thank Laboratorio Universitario de Cómputo de Alto Rendimiento (LUCAR) of IIMAS-UNAM for their service on information processing. We would like to thank the UNM Center for Advanced Research Computing, supported in part by the National Science Foundation, for providing the high performance computing resources used in this work.

Disclosures

The authors declare no conflicts of interest.

Data availability

The data that support the findings of this study are available from the authors upon request.

References

[1] Giovannetti, V., Lloyd, S., and Maccone, L. "Advances in quantum metrology". Nature Photon **5**, 222–229 (2011).

[2] Degen, C. L., Reinhard, F., and Cappellaro, P. "Quantum sensing". Rev. Mod. Phys. **89**, 035002 (2017).

[3] Hayashi, M. "Asymptotic theory of quantum statistical inference: Selected papers". WORLD SCIENTIFIC. (2005).

[4] Holevo, A. "Probabilistic and statistical aspects of quantum theory". Edizioni della Normale. (2011).

[5] Aasi, J., Abadie, J., and Abbott, t. "Enhanced sensitivity of the LIGO gravitational wave detector by using squeezed states of light". Nature Photon **7**, 613–619 (2013).

[6] Gatti, A., Brambilla, E., and Lugiato, L. "Chapter 5 Quantum imaging". Page 251–348. Elsevier. (2008).

[7] Kruse, I., Lange, K., Peise, J., Lücke, B., Pezzè, L., Arlt, J., Ertmer, W., Lisdat, C., Santos, L., Smerzi, A., and Klempt, C. "Improvement of an atomic clock using squeezed vacuum". Phys. Rev. Lett. **117**, 143004 (2016).

[8] Danilin, S., Lebedev, A. V., Vepsäläinen, A., Lesovik, G. B., Blatter, G., and Paraoanu, G. S. "Quantum-enhanced magnetometry by phase estimation algorithms with a single artificial atom". npj Quantum Inf **4** (2018).

[9] Gilchrist, A., Nemoto, K., Munro, W. J., Ralph, T. C., Glancy, S., Braunstein, S. L., and Milburn, G. J. "Schrödinger cats and their power for quantum information processing". J. Opt. B: Quantum Semiclass. Opt. **6**, S828–S833 (2004).

[10] Wiseman, H. M. and Milburn, G. J. "Quantum measurement and control". Cambridge University Press. (2009).

[11] Haroche, S. "Entanglement, decoherence and the quantum/classical boundary". Physics Today **51**, 36–42 (1998).

[12] Escher, B. M., de Matos Filho, R. L., and Davidovich, L. "Quantum metrology for noisy systems". Braz J Phys **41**, 229–247 (2011).

[13] Polino, E., Valeri, M., Spagnolo, N., and Sciarrino, F. "Photonic quantum metrology". AVS Quantum Sci. **2** (2020).

[14] Barbieri, M. "Optical quantum metrology". PRX Quantum **3**, 010202 (2022).

[15] Caves, C. M. "Quantum-mechanical noise in an interferometer". Phys. Rev. D **23**, 1693–1708 (1981).

[16] Maccone, L. and Riccardi, A. "Squeezing metrology: a unified framework". Quantum **4**, 292 (2020).

[17] Drummond, P. and Ficek, Z. "Quantum squeezing". Springer Berlin Heidelberg. (2004).

[18] Vahlbruch, H., Chelkowski, S., Danzmann, K., and Schnabel, R. "Quantum engineering of squeezed states for quantum communication and metrology". New Journal of Physics **9**, 371–371 (2007).

[19] Vahlbruch, H., Mehmet, M., Danzmann, K., and Schnabel, R. "Detection of 15 db squeezed states of light and their application for the absolute calibration of photoelectric quantum efficiency". Phys. Rev. Lett. **117**, 110801 (2016).

[20] Schönbeck, A., Thies, F., and Schnabel, R. "13db squeezed vacuum states at 1550nm from 12mw external pump power at 775nm". Opt. Lett. **43**, 110 (2017).

[21] Heinze, J., Willke, B., and Vahlbruch, H. "Observation of squeezed states of light in higher-order hermite-gaussian modes with a quantum noise reduction of up to 10 db". Phys. Rev. Lett. **128**, 083606 (2022).

[22] Berni, A. A., Gehring, T., Nielsen, B. M., Händchen, V., Paris, M. G. A., and Andersen, U. L. "Ab initio quantum-enhanced optical phase estimation using real-time feedback control". Nature Photon **9**, 577–581 (2015).

[23] Nielsen, J. A. H., Neergaard-Nielsen, J. S., Gehring, T., and Andersen, U. L. "Deterministic quantum phase estimation beyond N00N states". Phys. Rev. Lett. **130**, 123603 (2023).

[24] Lawrie, B. J., Lett, P. D., Marino, A. M., and Pooser, R. C. "Quantum sensing with squeezed light". ACS Photonics **6**, 1307–1318 (2019).

[25] Olivares, S. and Paris, M. G. A. "Bayesian estimation in homodyne interferometry". J. Phys. B: At. Mol. Opt. Phys. **42**, 055506 (2009).

[26] Monras, A. "Optimal phase measurements with pure Gaussian states". Phys. Rev. A **73**, 033821 (2006).

[27] Fujiwara, A. "Strong consistency and asymptotic efficiency for adaptive quantum estimation problems". J. Phys. A: Math. Gen. **39**, 12489–12504 (2006).

[28] Nagaoka, H. "On Fisher information of quantum statistical models". Page 113–124. WORLD SCIENTIFIC. (2005).

[29] Chiribella, G. and Mauro D'Ariano, G. "Extremal covariant measurements". J. Math. Phys. **47** (2006).

[30] Beneduci, R. "On the relationships between the moments of a POVM and the generator of the von Neumann algebra it generates". Int J Theor Phys **50**, 3724–3736 (2011).

[31] Keener, R. W. "Theoretical statistics: Topics for a core course". Springer New York. (2010).

[32] Braunstein, S. L. and Caves, C. M. "Statistical distance and the geometry of quantum states". Phys. Rev. Lett. **72**, 3439–3443 (1994).

[33] Helstrom, C. W. "Quantum detection and estimation theory". J Stat Phys **1**, 231–252 (1969).

[34] Glauber, R. J. "Coherent and incoherent states of the radiation field". Phys. Rev. **131**, 2766–2788 (1963).

[35] Aspachs, M., Calsamiglia, J., Muñoz Tapia, R., and Bagan, E. "Phase estimation for thermal Gaussian states". Phys. Rev. A **79**, 033834 (2009).

[36] Johnsson, M. T., Poggi, P. M., Rodriguez, M. A., Alexander, R. N., and Twamley, J. "Generating nonlinearities from conditional linear operations, squeezing, and measurement for quantum computation and super-Heisenberg sensing". Phys. Rev. Res. **3**, 023222 (2021).

[37] Zeytinoğlu, S., İmamoğlu, i. m. A., and Huber, S. "Engineering matter interactions using squeezed vacuum". Phys. Rev. X **7**, 021041 (2017).

[38] Weedbrook, C., Pirandola, S., García-Patrón, R., Cerf, N. J., Ralph, T. C., Shapiro, J. H., and Lloyd, S. "Gaussian quantum information". Rev. Mod. Phys. **84**, 621–669 (2012).

[39] Tyc, T. and Sanders, B. C. "Operational formulation of homodyne detection". J. Phys. A: Math. Gen. **37**, 7341–7357 (2004).

[40] Mauro D'Ariano, G., Paris, M. G., and Sacchi, M. F. "Quantum tomography". Page 205–308. Elsevier. (2003).

[41] Oh, C., Lee, C., Rockstuhl, C., Jeong, H., Kim, J., Nha, H., and Lee, S.-Y. "Optimal Gaussian measurements for phase estimation in single-mode Gaussian metrology". npj Quantum Inf **5** (2019).

[42] Genoni, M. G., Mancini, S., and Serafini, A. "General-dyne unravelling of a thermal master equation". Russ. J. Math. Phys. **21**, 329–336 (2014).

[43] Oh, C., Lee, C., Lie, S. H., and Jeong, H. "Optimal distributed quantum sensing using Gaussian states". Phys. Rev. Res. **2**, 023030 (2020).

[44] Lee, C., Lawrie, B., Pooser, R., Lee, K.-G., Rockstuhl, C., and Tame, M. "Quantum plasmonic sensors". Chem. Rev. **121**, 4743–4804 (2021).

[45] Holevo, A. "On the classical capacity of general quantum Gaussian measurement". Entropy **23**, 377 (2021).

[46] Silberfarb, A., Jessen, P. S., and Deutsch, I. H. "Quantum state reconstruction via continuous measurement". Phys. Rev. Lett. **95**, 030402 (2005).

[47] Wiseman, H. M. "Quantum trajectories and quantum measurement theory". Quantum Semiclass. Opt. **8**, 205–222 (1996).

[48] Martin, L. S., Livingston, W. P., Hacohen-Gourgy, S., Wiseman, H. M., and Siddiqi, I. "Implementation of a canonical phase measurement with quantum feedback". Nat. Phys. **16**, 1046–1049 (2020).

[49] Makelainen, T., Schmidt, K., and Styan, G. P. H. "On the existence and uniqueness of the maximum likelihood estimate of a vector-valued parameter in fixed-size samples". Ann. Statist. **9** (1981).

[50] Berry, D. W. and Wiseman, H. M. "Optimal states and almost optimal adaptive measurements for quantum interferometry". Phys. Rev. Lett. **85**, 5098–5101 (2000).

[51] Robert, C. P. and Casella, G. "Monte carlo statistical methods". Springer New York. (1999).

[52] Xiang, Y., Gubian, S., Suomela, B., and Hoeng, J. "Generalized simulated annealing for global optimization: The GenSA package". The R Journal **5**, 13 (2013).

[53] Ono, T. and Hofmann, H. F. "Effects of photon losses on phase estimation near the Heisenberg limit using coherent light and squeezed vacuum". Phys. Rev. A **81**, 033819 (2010).

[54] Lvovsky, A. I. "Squeezed light". Page 121–163. Wiley. (2015).

[55] Twamley, J. "Bures and statistical distance for squeezed thermal states". J. Phys. A: Math. Theor. **29**, 3723–3731 (1996).

[56] Liu, J., Yuan, H., Lu, X.-M., and Wang, X. "Quantum Fisher information matrix and multiparameter estimation". J. Phys. A: Math. Theor. **53**, 023001 (2019).

[57] Zhou, S. "Limits of noisy quantum metrology with restricted quantum controls" (2024). arXiv:2402.18765.

[58] Šafránek, D. and Fuentes, I. "Optimal probe states for the estimation of Gaussian unitary channels". Phys. Rev. A **94**, 062313 (2016).

[59] Huang, Z., Lami, L., and Wilde, M. M. "Exact quantum sensing limits for bosonic dephasing channels". PRX Quantum **5**, 020354 (2024).

[60] Holdsworth, T., Singh, V., and Wilde, M. M. "Quantifying the performance of approximate teleportation and quantum error correction via symmetric 2-PPT-extendible channels". Phys. Rev. A **107**, 012428 (2023).

[61] Hayashi, M. and Ouyang, Y. "Finding the optimal probe state for multiparameter quantum metrology using conic programming" (2024). arXiv:2401.05886.

[62] Xu, C., Zhang, L., Huang, S., Ma, T., Liu, F., Yonezawa, H., Zhang, Y., and Xiao, M. "Sensing and tracking enhanced by quantum squeezing". Photon. Res. **7**, A14 (2019).

[63] DiMario, M. T. and Becerra, F. E. "Demonstration of optimal non-projective measurement of binary coherent states with photon counting". npj Quantum Inf **8** (2022).

[64] DiMario, M. T. and Becerra, F. E. "Channel-noise tracking for sub-shot-noise-limited receivers with neural networks". Phys. Rev. Res. **3**, 013200 (2021).

[65] Paninski, L. "Asymptotic theory of information-theoretic experimental design". Neural Comput **17**, 1480–1507 (2005).

[66] Belsley, A., Allen, E. J., Datta, A., and Matthews, J. C. F. "Advantage of coherent states in ring resonators over any quantum probe single-pass absorption estimation strategy". Phys. Rev. Lett. **128**, 230501 (2022).

[67] DiMario, M. T. and Becerra, F. E. "Single-shot non-Gaussian measurements for optical phase estimation". Phys. Rev. Lett. **125**, 120505 (2020).

[68] Rodríguez-García, M. A., DiMario, M. T., Barberis-Blostein, P., and Becerra, F. E. "Determination of the asymptotic limits of adaptive photon counting measurements for coherent-state optical phase estimation". npj Quantum Inf **8** (2022).

[69] Pope, D. T., Wiseman, H. M., and Langford, N. K. "Adaptive phase estimation is more accurate than nonadaptive phase estimation for continuous beams of light". Phys. Rev. A **70**, 043812 (2004).

[70] McCormick, W. P., Mallik, A. K., and Reeves, J. H. "Strong consistency of the MLE for sequential design problems". Stat. Probab. Lett. **6**, 441–446 (1988).

[71] Rudin, W. "Principles of mathematical analysis". International series in pure and applied mathematics. McGraw-Hill Professional. New York, NY (1976). 3 edition.

[72] Williams, D. "Probability with martingales". Cambridge University Press. (1991).

[73] Chung, K. L. and Erdös, P. "On the application of the Borel-Cantelli lemma". Trans. Am. Math. Soc. **72**, 179–186 (1952).

[74] Bishop, Y., Light, R., Mosteller, F., Fienberg, S., and Holland, P. "Discrete multivariate anal-

ysis: Theory and practice". Springer New York. (2007).